September 2021

Zeta Potential Measurements For Surface Modification Of Plastic Substrates For Nanofluidic Biosensors

Qinhan Liu
Louisiana State University and Agricultural and Mechanical College

ZETA POTENTIAL MEASUREMENTS FOR SURFACE MODIFICATION OF PLASTIC SUBSTRATES FOR NANOFLUIDIC BIOSENSORS

A Thesis

Submitted to the Graduate Faculty of the
Louisiana State University and
Agricultural and Mechanical College
in partial fulfillment of the
requirements for the degree of
Master of Science in Mechanical Engineering

in

The Department of Mechanical Engineering

by
Qinhan Liu
B.S. Huazhong University of Science and Technology, China, 2017
December 2021

ACKNOWLEDGMENTS

I would first like to thank my advisor, Dr. Sunggook Park, for his kindest support and patience throughout my graduate studies. His invaluable guidance and insights helped me to become a better researcher. I would also like to express my gratitude to Dr. Junseo Choi for all his advice and guidance on my research and career planning. I am deeply grateful for his time and effort in teaching me the details of my experiments.

I would like to acknowledge Dr. Daniel Park, Dr. Michael C. Murphy, and Dr. Steven Soper for their collaboration in this project. And I am really appreciated all the members of my research team, Ramin Riahipour, Daewon Kim, Dr. XiaoXiao Zhao, for their research support and friendship.

Besides, I would like to thank Dr. Dorel Moldovan and Dr. Manas Gartia for agreeing to serve as my committee members.

Finally, I give my deepest gratitude to my families and friends, whose understanding and psychological support has meant a lot to me. Thank you for every step along the way.

Table of Contents

ABSTRACT

Polymeric materials have revealed their great potentials in micro- and nano- fluidic devices for biosensing. Their advantages include low cost, various physicochemical properties, well-developed fabrication, and surface modification protocols comparing with traditional materials such as silicon or glass. Surface modification consists an essential step in fabrication of polymer-based biosensors. A proper characterization is required to justify the effectiveness of modifications on polymer surface.

For nanofluidic devices, special phenomena such as overlapped electrical double layer, ion rectification and electroosmosis flow can dominate the behavior of single molcules. The concept of surface charge density plays a key role in nanofluidic devices due to its effects on electrophoresis and electroosmosis in the nanostructures. For example, a polymeric materials with low surface charge density is preferred for DNA translocation. Thus, the measurement technique of surface charge density is promising to select a proper material for nanofluidic sensor and assess the performance of polymer after surface modification.

This work presents zeta potential measurements on PMMA, a common thermoplastic polymer, which is treated by UV/Ozone irradiation, O_2 plasma, covalent crosslinking of 3-(3-dimethylaminopropyl) carbodiimide/N-hydroxysuccinimide (EDC/NHS). And determine the optimal surface activation protocol via monitoring zeta potentials for different treatment conditions. Finally, lambda-Exonuclease (λ-Exo) will be anchored on the EDC/NHS functionalized PMMA surfaces and the effectiveness of binding biomolecule will be studied.

Chapter 1. Introduction

1.1. General background

Nanofluidic devices, applying fluid flow with at least one dimension below 100nm, are one of the research interests for decades. The nanometric dimension provides several unique features, including high surface-to-volume ratio, entropic barriers, comparable surface charge, ion-current rectification, length scale of important biomolecules like DNA strands.[1–3] Those features give access to explore novel scientific phenomena and inspire a wide range of applications in physical, chemical, and biological fields. With advances in nanofabrication technologies, various well-defined nanometric geometries are designed to study nanoscale reaction, fluidic properties of DNA or other properties.[4]

Nanosized pores can be used to take biomolecule detection for DNA, RNA or proteins. With the identical ionic current activated by translocations of charged molecules through nanopore, the rapid, high-resolution and real-time DNA sequencing comes true.[3, 5] Such development of bio detection will advance people's understanding of genetics and open up many possibilities. For example, a growing recognition among health providers in decades is that the genetic-based, accurate and personalized treatment, named precision medicine, has the prospect to maximize medical outcomes and minimize cost, especially for a highly heterogeneous disease like cancer, where different treatment options for different people can help improve patient prognosis.[6]

Polymer-based nanofluidic devices attract the interest of researchers for their advantages such as high optical transparency, low-cost fabrication method with good fidelity and a wide range of chemical properties.[7] However, polymers are inherently hydrophobic with smaller functional groups compared to conventional materials such as glass or silica.[8] To meet

requirements regarding adhesion, wettability, biocompatibility, and nonspecific adsorption, surface modification is essential for polymer-based nanofluidic devices.

Moreover, surface modification techniques help nanoscale biosensors overcome the difficulty in controlling molecule motion. Slowing down the translocation of single molecule can increase the signal-to-noise ratio.[9, 10] The function of bioreactor combined with nanofluidic sensors via modification treatment also assist in the high-resolution identification.[11]

The characterization method, zeta potential measurement, reflects the electrical potential near the surface of the polymeric substance after surface modifications. Since there are not many systematic works done regarding the zeta potential under the influence of surface modifications. In this thesis, we are going to measure zeta potential for a series of surface-treated polymers and reveal their electrokinetic behaviors.

1.2. Goals and objectives

The goal of this thesis is to systematically study the change of zeta potentials upon surface functionalization protocols that have routinely been applied to modify polymer surfaces widely used in plastic nanofluidic biosensors.

This work focuses on poly(methyl methacrylate) (PMMA), a thermoplastic polymer widely known as plexi-glass. PMMA is the plastic that has most widely used for microfluidic applications due to the low cost, high optical transparency, and availability of high throughput manufacturing methods including imprinting (hot embossing) and injection molding. The surface functionalization protocol that is exploited in this study is the 3-(3-dimethylaminopropyl) carbodiimide/N-hydroxysuccinimide (EDC/NHS) coupling chemistry modification, which consists of surface activation process using either O_2 plasma treatment or UV/O_3 treatment of PMMA surface followed by the sequential or concurrent binding of EDC and NHS. The EDC/NHS modification provides a useful linker leading to stable binding of many biological reagents to solid substrates[12, 13] including enzymes and fluorescent dyes.

The objectives of this work to achieve the research goal are as follows:

(1) To monitor zeta potentials for O_2 plasma and UV/O_3 treatments under different conditions to identify the optimal surface activation protocol on PMMA substrate.

(2) To measure zeta potentials upon the EDC/NHS functionalization on differently activated PMMA substrates to determine the ideal combination of surface activation and EDC/NHS modification protocols.

(3) To study the effectiveness of binding biological reagents on the EDC/NHS functionalized PMMA surfaces.

1.3. Outline of the manuscript

There are four chapters in this thesis. The summary of each chapter is given below.

Chapter 1 covers a preview of this thesis and the goal and objectives of this study.

Chapter 2 shows the literature review of important phenomena in nanofluidic devices, measurement methods and the surface modification techniques.

Chapter 3 describes the details of those experiments including surface treatments and characterization methods.

Chapter 4 provides characterization results on surface activated PMMA after UV/O_3 and O_2 plasma treatments separately.

Chapter 5 shows the effectiveness of the covalent bonding on PMMA. Chemical intermediates of EDC/NHS and fluorescein are anchored to the physically activated PMMA samples step by step.

Chapter 6 reveals the zeta potential measurement results of λ-Exo immobilized PMMA with different time conditions.

Chapter 7 concludes the key descriptions in this research as well as an outline for future work.

Chapter 2. Literature review

In this chapter, literature will be reviewed regarding to nanofluidic systems. First, the important physical concepts about electrokinetic phenomena inside nanofluidic platforms will be introduced, as well as their influence on transportation behaviors. Second, the understanding about zeta potential and surface charge density will be introduced, followed by the measurement methods for flat samples. Thirdly, the surface modification techniques of nanofluidic devices will be covered.

2.1. Electrokinetic phenomena in nanofluidic systems

2.1.1. Introduction to physical concepts of nanofluidic systems

At the nanoscale, unique physical phenomena, such as surface charge, double layer overlap, and ion current rectification, can affect the transportation behaviors, which are ignorable or insignificant in microscale fluidic devices. Here some basic definitions will be introduced as the starting points to understand unique phenomena inside nanofluidic systems.

The electric double layer (EDL) is an important concept for nanofluidic devices in terms of colloidal systems and electrode-solution interfaces. As a charged solid surface contacts with an aqueous solution, EDL is developed from oppositely charged ions in solution, which rearranged themselves and adhered to the solid-liquid interface to maintain electrical neutrality. Such balancing counterions in the liquid is referred to as the EDL. There are two layers in EDL. The first region is the Stern layer where counterions experience strong electrostatic forces and are considered to be immobile. The second layer of ions located outside the Stern layer is called the diffuse layer, which is the relatively mobile layer due to a weaker electrostatic attraction. the shear plane is defined as the boundary separating these two layers. The concentration of ions will decrease gradually with distance to the surface until it reaches the bulk concentration.

Debye length ($\lambda_D = \kappa^{-1}$) is the parameter to characterize the thickness of EDL, which is the distance from the charged surface where the potential has decayed to the 1/e point or 36.7% of the surface potential.[14] The thickness of EDL depends on salt concentrations and surface charge density, which is typically on the order of 1−30 nm.[15] Fig 2.1 is the schematic illustration of an EDL.

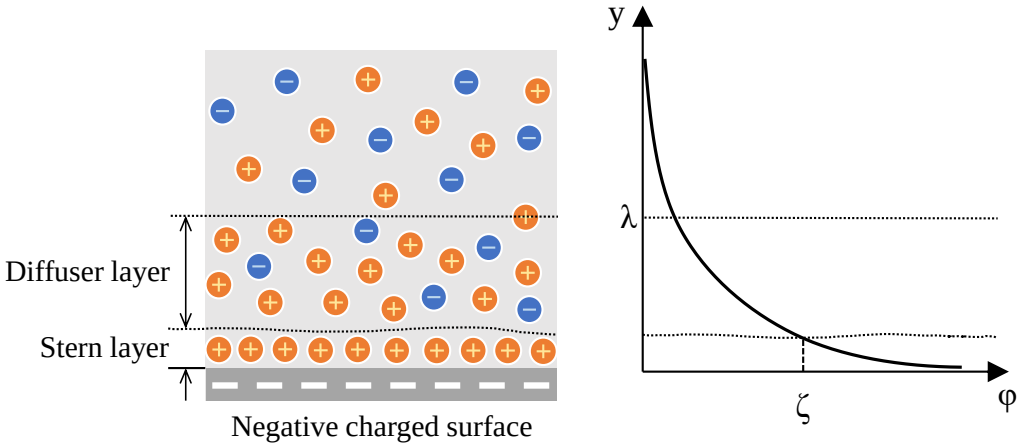

Figure 2.1. Schematics of the ionic concentration and the potential field in an electric double layer.

In nanofluidic systems, driving flow simply by pressure is impractical. Electric fields generated by electric potential or external voltages are more commonly used. There are various electrokinetic effects, and the four primary kinds in nanofluidic systems are:

Electroosmosis is defined as the liquid motion relative to a stationary charged surface. The direction of electroosmotic flow can be different from the direction of bulk flow.

Electrophoresis is defined as the motion of charged particles in a fluid under the influence of an electric field.

Streaming potential is defined as an induced electrokinetic potential in a flow driven by external forces such as pressure through a charged surface. This concept is the opposite concept of electroosmosis.

Sedimentation potential is defined as the induced electric field when charged surfaces or particles move with respect to stationary fluid. This phenomenon is the opposite of electrophoresis.

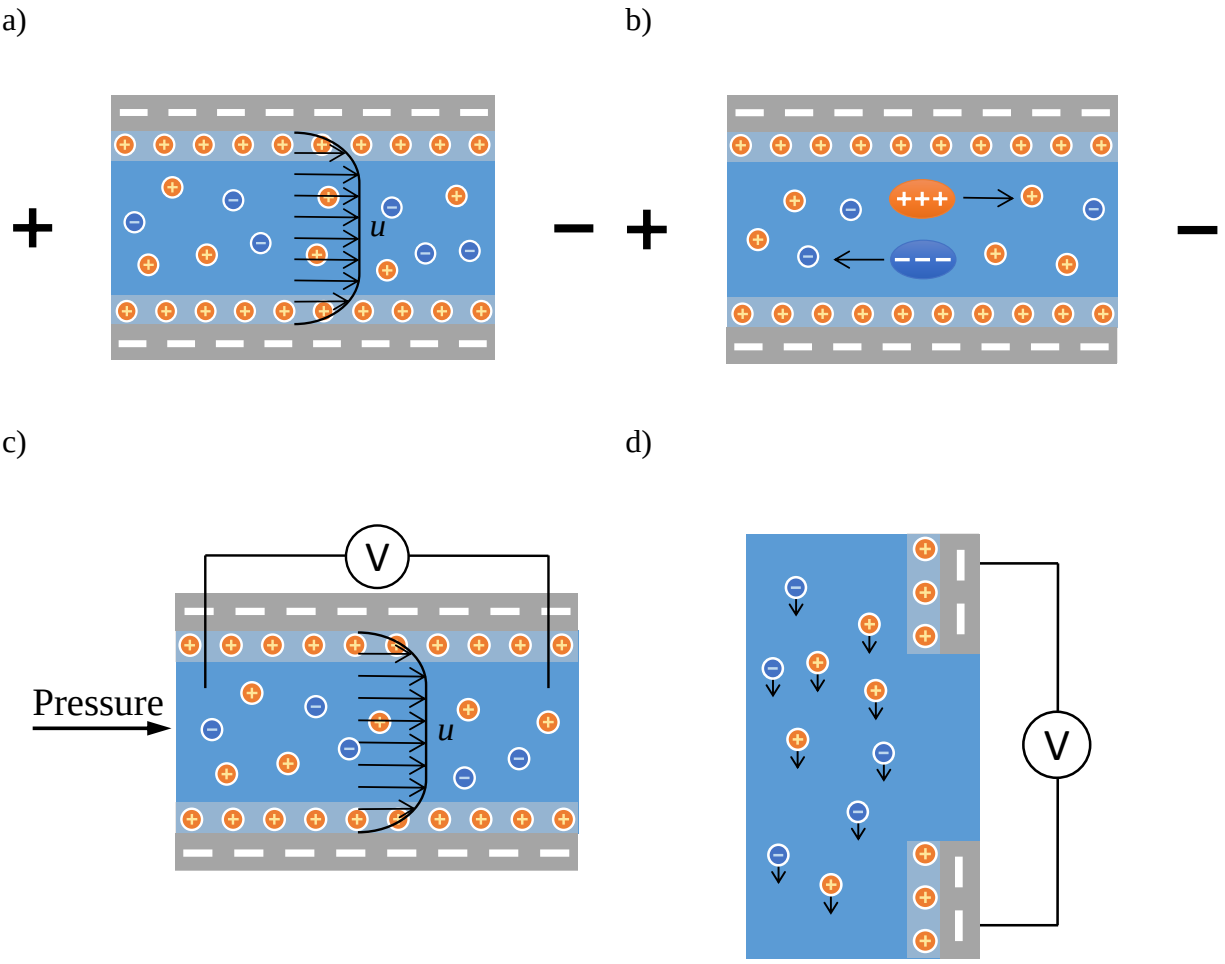

Figure 2.2. Schematics of electrokinetic phenomena in a negatively charged nanochannel: (a) electroosmosis; (b) electrophoresis; (c) streaming potential; and (d) sedimentation potential.

2.1.2. Theoretical development on the electrokinetic behaviors of nanofluid

Since electrokinetic effects significantly impact transport through nanofluidic structures, developing proper theories to predict their roles is in great of interest. From 1960s, researchers have noticed electroosmotic flow (EOF) in a nanochannel is influenced when the electrical double layer extends into the channel at low salt concentrations, and result in a reduced velocity.[16, 17] Physical factors influence on EOF have been investigated theoretically and showed the potential to control EOF. Yeh et al. controlled surface-charge property as well as EOF by the nanofluidic field-effect transistor.[18]

The electrophoretic mobility of charge species is proven to be dependent on particles mobility and the shape of the electric double layer.[19, 20] At high pH, the particle behavior may dominated by EOF and alter the direction of electrophoresis.[21].

The analytical solutions describing the sedimentation velocity and sedimentation potential were derived by Keh et al. in terms of charged composite spheres, charged soft spheres and charged porous spheres under the requirement of zero net electric current.[22–24]

Because the generation of electric streaming current attributes to the movement of ions in the bulk and EDL, it was found to be reduced by double layer overlap and the approximation of it required corresponding correction factors.[16] Recent work provided analytical solutions to quantify streaming potential and electroviscous effects in nanocapillary, in which three distinct regimes of streaming potential were demonstrated corresponding to the influence of the EDL thickness that depend on conduction current.[25] Bandopadhyay et al adjust the simulations of streaming potentials via taking the size effects in the ion distribution profile into account, which give rise to the streaming potential predictions.[26, 27]

2.2. Zeta potential and surface charge density

2.2.1. Introduction of zeta potential and surface charge density

Since the behaviors of nanofluidic systems are essentially affected by electrostatic and electrokinetic effects, characterizations of them in proper methods become necessary to design effective nanofluidic device for specific applications. Zeta potential (ζ) and surface charge density (σ) are two impactful parameters to study and model a variety of electrokinetic performance in the system.

Zeta potential refers to the electrical potential at the shear plane of the electric double layer. It is unique for each solid-liquid interface for the reason that the zeta potential depends on a number of factors including the ion concentration, ion valence, pH value, surface roughness and temperature of the solution. Measurement of zeta potential are indirect readings obtained from electrokinetic experiments.

Surface charge density is difficult to be measured during experiments. Therefore, it is evaluated based zeta potential.

2.2.2 Methods to zeta potential and surface charge density measurement in slit.

Three main techniques of zeta potential measurements base on electroosmotic flow, electrophoresis and streaming potential separately, where electroosmotic and streaming potential methods are adopted in the study of microchannel. Since electrophoresis methods are used for charged particles which is not related to our polymer-based nanofluidic devices, I will only introduce the other two methods in this section.

In electroosmotic flow, the motion of ions is affected by EDL, and results in a plug-like velocity profile, where the velocity is zero at the solid-liquid interface and rises to a uniform bulk velocity. Since the EDL thickness is very small (around 30nm) compared a microscale channel,

the edge effects can be minimized and lead to a uniform velocity along the height of the channel. Under this condition, the average electroosmotic flow velocity is given by the classic Helmholtz-Smoluchowski equation[28]:

$$v_{av} = \frac{\epsilon_r \epsilon_0 \zeta}{\eta} E_z \qquad (2.1)$$

where ϵ_o is the permittivity of the vacuum, ϵ_r is the dielectric constant of water, at 25℃, η is the solution viscosity, E_z is the electric field and ζ is the zeta potential. The group of terms $\frac{\epsilon_r \epsilon_0 \zeta}{\eta}$ is called the electroosmotic mobility (μ_{eo}). This equation can determine the zeta potential by measuring the fluid velocity in a microchannel under electroosmotic flow.

As for streaming potential method, a pressure-driven electrolyte solution through a microchannel creates a potential difference, known as the streaming potential. This potential makes an electric force in the opposite direction of the liquid flow. For a charged flat solid surface which is isolated enough, the streaming current is given by[29]:

$$I_{str} = \frac{\Delta P \epsilon_r \epsilon_0 \zeta A}{\eta L} \qquad (2.2)$$

where A is the cross-sectional area, ΔP is the pressure difference and L is the distance of the channel in the direction of the liquid flow. In our experiment, the zeta potential of planar surface with known geometry can be calculated via equation (1.2), which requires only one measured parameter ($\frac{dI_{str}}{d\Delta P}$) with reduced measurement errors[30]. Figure 2.3 shows a schematic representation of the solid materials with planar surfaces for the zeta potential measurement. For practical purposes, other streaming potential experiments are performed with different factors to increase the accuracy of the measurements.

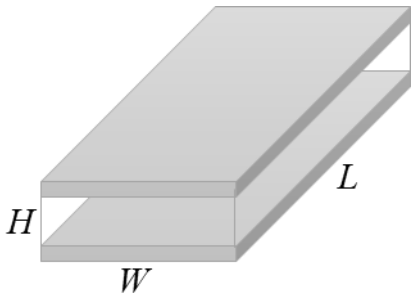

Figure 2.3. Schematic figure of the arrangement of flat surfaces for zeta potential measurement.

In the planar limiting case, as the zeta potential and ionic strength are known, the surface charge density can be calculated by Grahame equation[31]:

$$\sigma_\zeta = \frac{2\epsilon_r \epsilon_0 k_B T}{e\lambda_D} \sinh\left(\frac{e\zeta}{2k_B T}\right) \qquad (2.3)$$

, where e is the elementary charge, k_B is the Boltzmann constant and T is the room temperature.

2.3. polymer nanofluidic devices

Nanopore structure is widely existed in nature, such as re alpha hemolysin, aerolysin, and MspA porin. However, biological nanostructures have their limitations regarding stabilities and size[32, 33]. To undertake complex applications of nanofluidic systems such as biomolecule monitoring and chemical analyses, inorganic substrates such as silicon dioxide[34, 35], silicon nitride [9, 36, 37], and glass capillaries[38–40] are developed in recent years for their advantages in surface chemistry, optical properties and stability. The fabrication methods include focus ion beam, electron beam lithography, wet/dry etching, laser pulling, etc.

Polymers are advance materials to fabricate nanofluidic devices. Compared to silicon and glass materials, polymers have lower material costs, a wide range of physiochemical properties and diverse protocols of fabrication and surface modification[7]. In general, polymers are categorized as elastomers and thermoplastics. Elastomers are amorphous polymers with low Young's moduli and high failure strain. On the other hand, thermoplastics have higher molecular weights and Young's moduli. Polydimethylsiloxane (PDMS) is a common elastomeric material with applications in nanofluidic devices[41, 42]. While poly(methylmethacrylate) (PMMA), polycarbonate (PC); and cyclo-olefin-copolymer (COC) are thermoplastic examples. Because of the low Young's modulus of elastomers, nanostructure collapse may occur during thermal/pressure operation such as assembly process. Moreover, elastomers hardly allow the pioneering fabrication method, nanoimprint lithography (NIL) to be applied. As figure 2.4 shows, NIL has been demonstrated to fabricate sub-10 nm scales with the ultimate resolution and fidelity[43]. And thermoplastic shares such advantages of NIL about production of complex multi-scale structures repetitively over large areas at low-cost.

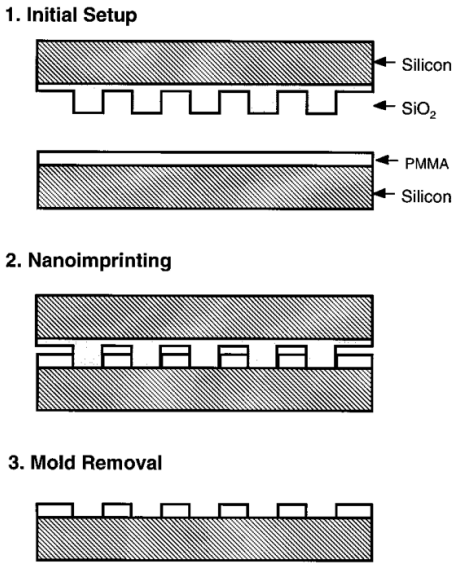

Figure 2.4. Schematic of nanoimprint lithography process.[43]

Based on the previous research conducted by Daewon Kim, PMMA, among five common-used thermoplastics for nanofluidic biosensors, showed the lowest absolute value of electrokinetic surface charge density and the variance of each measurements was low. Hence, PMMA has higher potential in biomolecule sensing. The relatively stable measurement results also make it promising regarding the characterization methods in this paper.

2.4. Surface modification on polymer-based nanofluidic devices

Although polymers are attractive materials to form nanofluidic devices, they are innately hydrophobic, which means polymers is difficult to bind different materials robustly and tends to adsorb hydrophobic analytes. Moreover, the negligible presence of ionizable functional groups in polymers produce much smaller EOF compared to glass-based devices[8]. Thus, the surface of polymers must be modified to meet requirements regarding wettability, biocompatibility, and nonspecific adsorption. There are various surface modification protocols, such as plasma[44–50], corona[51–53], UV or UV/ozone irradiation[53–58], photografting and chemical methods of surface modification[59–63] etc.

2.4.1. Surface activation of polymers by O2 plasma treatment

O_2 plasma treatment is a common method to functionalize polymer surface, alter the wettability behavior, increase adhesion between different substance.

O_2 plasma treatment was conducted by reactive-ion etching (RIE) system. After placing the samples in the cylindrical vacuum chamber, the chamber was reached to a low pressure. O_2 enters the chamber from small inlets on the top and exits to the vacuum pump through the bottom of the chamber. As the power provided to the system, the O_2 plasma particles impact the polymer surface as well as increase surface roughness.[64]

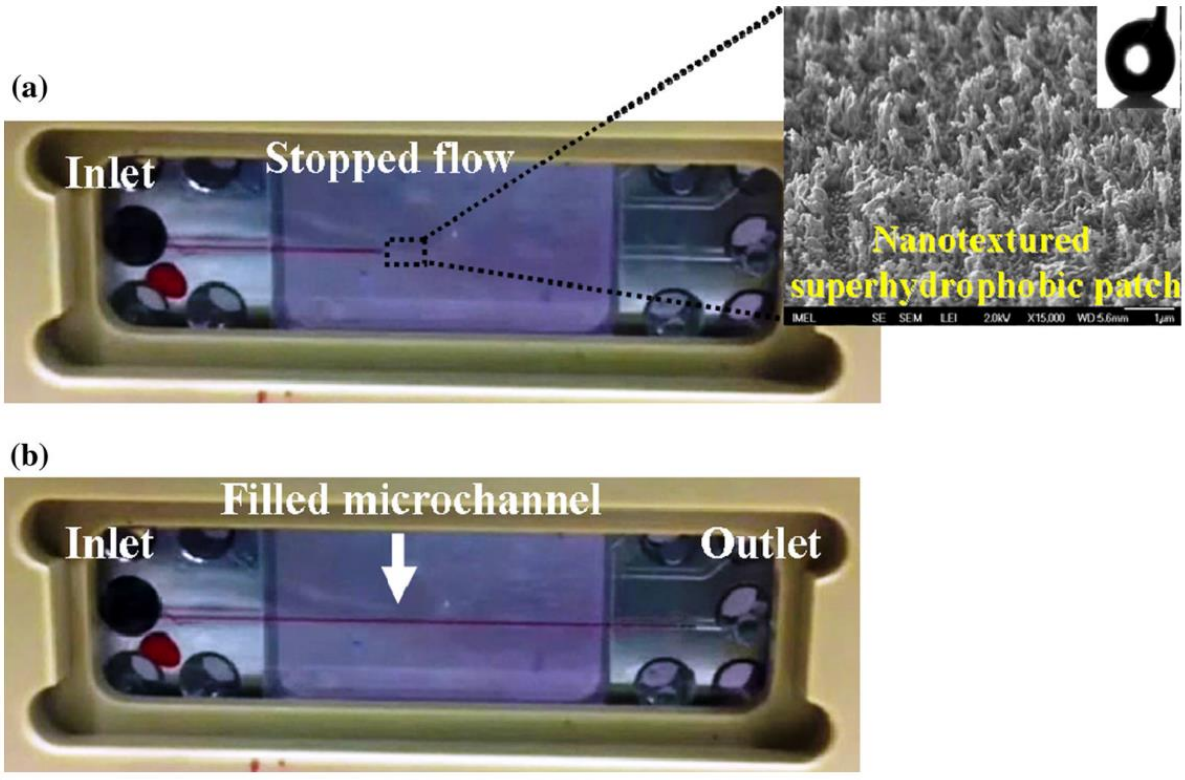

Figure 2.5. image of a passive superhydrophobic microvalve in the middle of the microchannel and its SEM image.[65]

Sunkara et al.[59] described a room temperature bonding method of various thermoplastics, PMMA, PC, COC and PS to PDMS. They activated thermoplastics by oxygen

plasma to produce oxhydryl group followed by aminopropyltriethoxysilane (APTES) modification. The treated thermoplastics were then brought to plasma treated PDMS at room temperature for assembly. The enclosed devices showed high burst resistance and hydrolytic stability.

Ellinas et al.[65] presented a nanotextured PMMA manipulated via O_2 plasma etching, that PMMA with rough surface became superhydrophobic, which could split the liquid flow and were test as superhydrophobic valves (figure 2.5.) to deliver fluids in an analytical device in a preferred sequence.

2.4.2. Surface activation of polymers by UV/O3 treatment

The role of UV/O_3 radiation is usually overlapped with O_2 plasma treatment. UV/O_3 radiation utilized the effects of UV light (< 254 nm) to produce in situ ozone from a gas-phase photodissociation of molecular oxygen. The formation or decomposition of O_3 with ultraviolet rays generates atomic oxygen O, which has strong oxidizing ability. Atomic O, along with ultraviolet rays, break the polymer chain by insertion of oxygen-containing functional groups. As a result, surface energy and oxygen levels of the polymers were increased.

Tsao et al. demonstrated the enhancement of UV/O_3 treatment on bond strength for PMMA and COC at low temperature. Though the initial dimensions of PMMA microchannels were same, the channel collapsed for the bonded PMMA without 24min UV/O_3. Figure 2.6. compared the wall deformation of PMMA through two bonding strategies.[56]

The carboxyl acid is the dominate specie on PMMA and COC following by UV/O_3 treatment, which increased wettability of the surface and played as desired scaffolds for following covalent attachment of biologics. Jackson et al. utilized UV/O_3 treated COC with anchored antibodies for circulating tumor cell (CTC) analysis.[66]

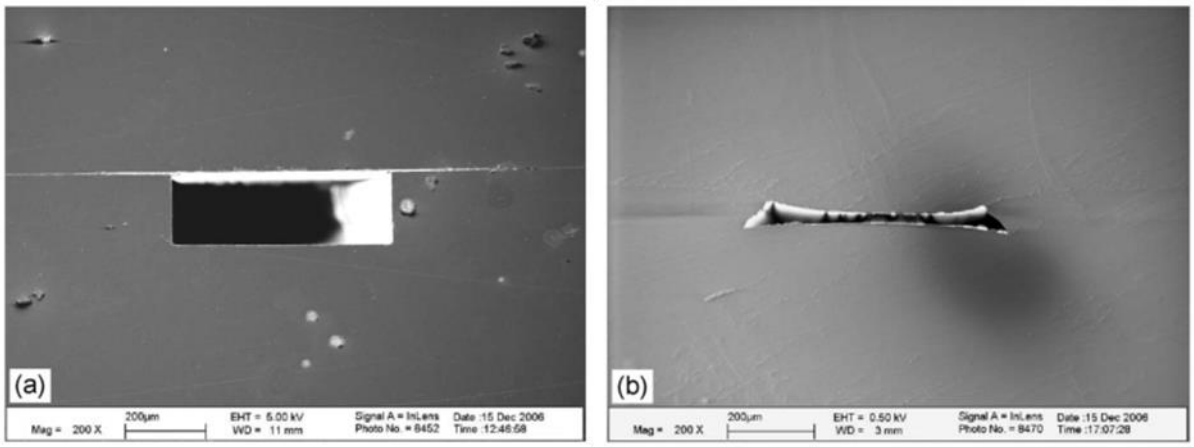

Figure 2.6. SEM image of 500 mm wide, 180mm deep PMMA microchannels following (a) thermal bonding of 24 min UV/O_3 treated PMMA substrates at 60℃, and (b) thermal bonding of virgin PMMA substrates at 100 ℃.[56]

2.4.3. Surface functionalization via EDC/NHS treatment

EDC/NHS coupling chemistry is commonly used to conjugate biological substances containing carboxylates and amines. EDC is a water-soluble zero-length crosslinker, which allows to form a bond without additional atoms or spacing. Since EDC is labile in the presence of water, the bulk chemical must be stored at −20°C. Figure 2.7(a) is the preferred route about how amide bond is formed in aqueous solution. Except the desired conjugation product, a number of potential side products can be generated, including undesired inactive isourea that no longer can participate in the reaction process.

On poly(methacrylic acid) (PMAA) grafted on silicon, Wang et al. confirmed a different EDC activation mechanisms related to an anhydride intermediate. This side product formed from a carboxylate group and a neighboring *O*-acylisourea ester also has reactivity with amine groups. Because polymers contain repeating carboxylate groups, it is possible that the anhydrides become the primary intermediate reactive group formed from EDC[67].

(a)

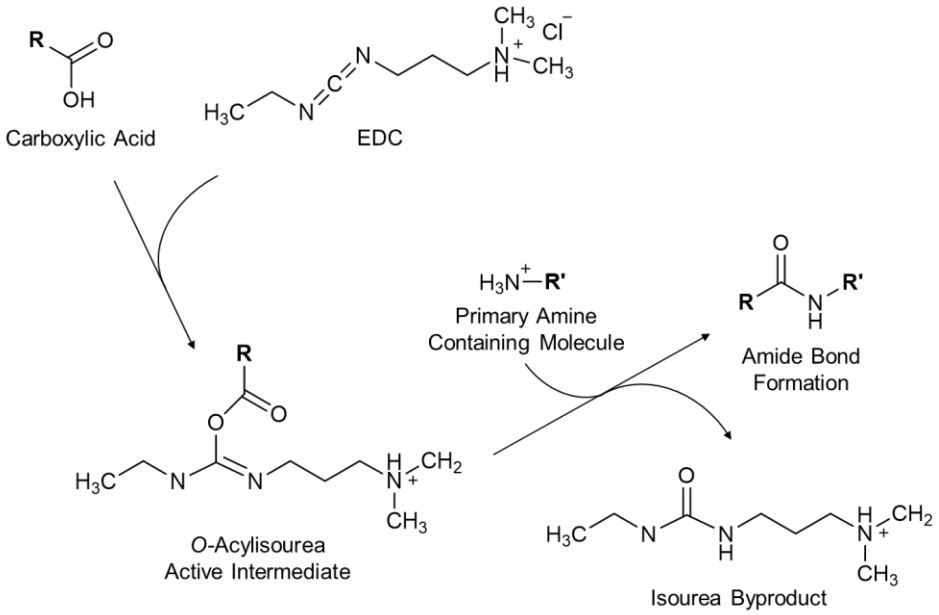

(b)

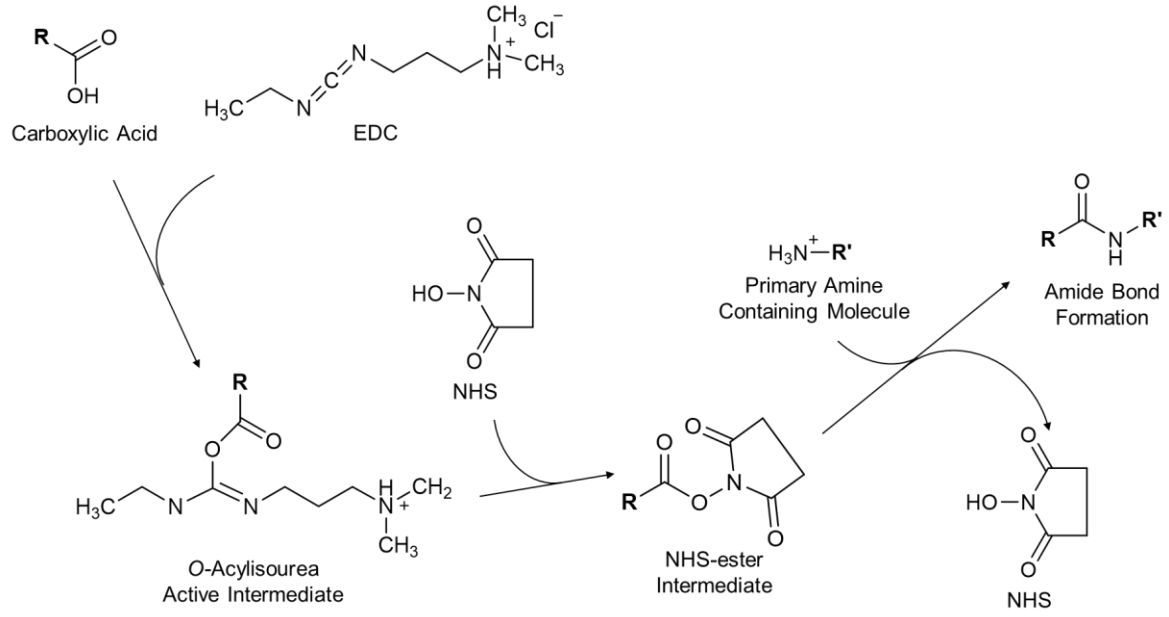

Figure 2.7. conjugation reaction between carboxylic acids and amine-containing molecules in the presence of (a) EDC only; (b) EDC and NHS**[68]**.

Usually, EDC combining with NHS or sulfo-NHS is a universal way to improve the solubility and stability of the active intermediate, which ultimately reacts with the attacking amine[69]. As the figure 2.7(b) shows, after EDC reacts with a carboxylate group to form an *O*-

acylisourea active ester, succinimidyl ester groups from the reaction of the hydroxyl group on NHS with the EDC active-ester complex replace the previous active intermediates. However, the increased efficiency obtained by the use of NHS may result in a severe precipitation during the reaction. In that case, eliminating NHS or sulfo-NHS can preserve the solubility of the final product.

As mentioned before, EDC/NHS is used frequently to conjugate substances containing carboxylates and amines. Many potential medical applications were being developing with assistance of EDC/NHS treatment, such as CTC analysis performed on antibody anchored COC devices[66], DNA or RNA sequencing on enzyme immobilized PMMA[11, 70] and drug delivery with fibroin-based nanoparticles utilizing crosslinker EDC (EDC-FNPs).[71] Keleştemur et al.[69] utilize EDC/NHS to reduce cytotoxicity of the original ZnO nanoparticles via covalent attachment of bovine serum albumin (BSA). EDC/NHS also aid in modification of liquid permeability of nanofiltration (NF) membranes[13, 72].

2.5. Binding of Enzyme on polymer surfaces

Microfabricated analytical devices have been developed for decades. Recently, a novel microfluidic analytical systems became attractive. Such microfluidic devices can accomplish biological reactions via enzyme immobilization, which is named as Immobilized Microfluidic Enzymatic Reactors (IMERs). The integration of an enzyme in a microchip bring several advantages. First, IMER can increase system automation as well as eliminate errors associated with manual protocols[73]; besides, it can be coupled with numerous detection techniques for biomedical applications such as glucose measurements[74]. IMER also enhanced reaction efficiency due to reduced diffusion distances, a reduction of analysis time and sample consumption. For example, magnetic nanoparticles or microparticles with immobilized enzyme

offer a manipulation method to control enzymes magnetically and generate specific organized structures for digesting proteins efficiently.[75, 76]

The functions of immobilized enzymes limit the potential applications of IMER. Except the enzymes on in industry, such as glucose isomerase, sucrose mutase, h-galactosidase and penicillin acylase[77], more enzymes are studied for IMERs. By covalent attachment of enzymes, polymeric materials, PMMA[11, 70, 78] and COC[70], are successfully utilized to fabricate IMERs.

Athapattu et al. immobilized exoribonuclease-1(XRN1) immobilized within a PMMA-based microfluidic device. Since XRN1 cleaves ssRNA in the 5’ to 3’ direction, this IMER is potential in single-molecule RNA exosequencing.[11]

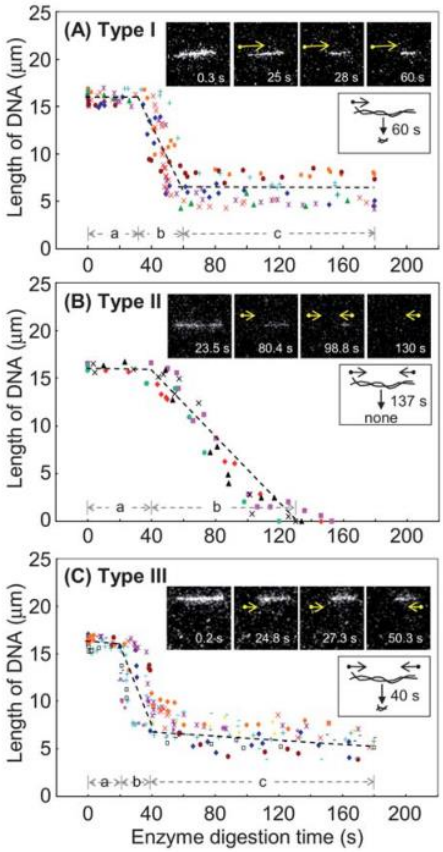

Figure 2.8. Different digestion modes based on the decrease in the length of the single-DNA molecules by lambda-exonuclease at the interface of the buffer solution and the fused-silica prism.[79]

To realize DNA sequencing, lambda-exonuclease (λ-Exo) was chosen.[70] λ-Exo is an ATP-independent enzyme which can processively digest the 5′-ended strand of double-strand DNA(dsDNA) to form 5′ mononucleotides in free-solution as well as generate an intact ssDNA byproduct[80]. The λ-Exo digestion rates of entrapped DNA molecules in solid-state nanopores was previously studied by Lee et al.[81, 82] As reported, the enzyme digestion rates was strongly affected by the geometry, functional groups in confined nanopores. Kang et al. observed three digestion modes of the single-DNA molecules by λ-exonuclease at the solid-liquid interface (Figure 2.8): incomplete digestion at one end with a small spot remained; complete digestion from both ends and incomplete digestion from both ends.[79]

Inspired by previous reports,[83, 84] immobilized λ-Exo in biosensor was studied in application of the sequence analysis of DNAs. The strategy is that individual nucleotide molecules cleaved by exonuclease enzyme could be identified in correct order through an appropriate detection method such as time of flight in nanochannel. Oliver-Calixte et al. initially immobilized λ-Exo to PMMA-based IMER via EDC/NHS coupling chemistry, which were shown in figure 2.9.[70] The calculated average digestion rate was 1000 ± 100 nucleotides per second(nt/s), and the processivity was over 40 kbp which was significantly higher than the free solution enzyme. Their conclusion suggested a promising application of enzyme immobilized lab-on-chip devices with enhanced enzymatic activity and stability.

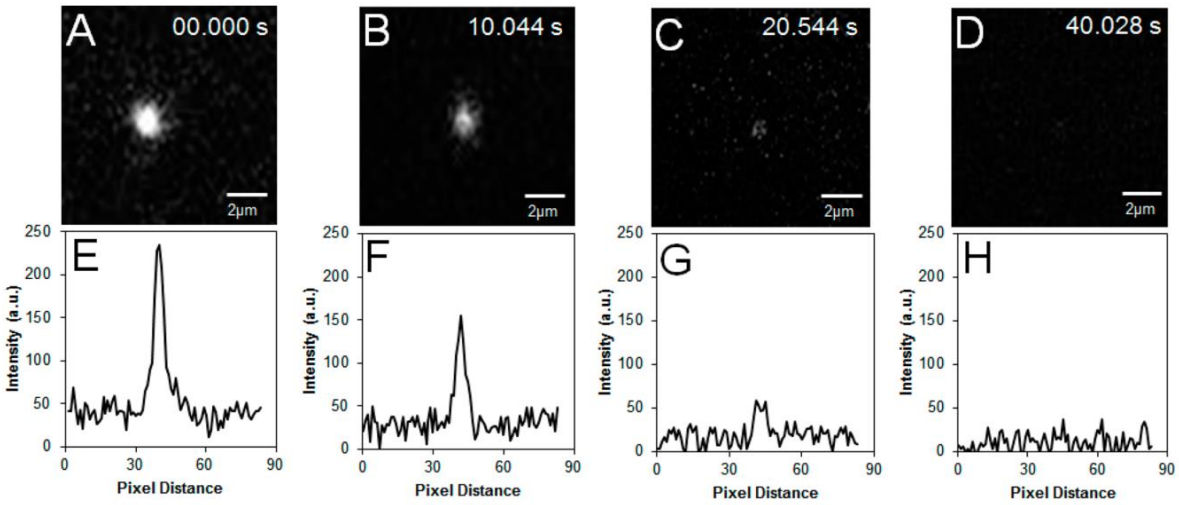

Figure 2.9. (A−D) Fluorescence still images for the real-time digestion of dsDNA using λ-Exo covalently immobilized to a PMMA substrate configured in the IMER device. (E−H) The corresponding fluorescence intensity line plots taken from the still images shown in parts A−D. [70]

Chapter 3. Methods

3.1. Materials

The polymer used in this study is 10 mm × 20 mm poly(methyl methacrylate) (PMMA), which was purchased from ePlastics. Bulk EDC, NHS, APTES and BupH™ MES Buffered Saline Packs, which were used to prepare MES buffer were purchased from ThermFisher Scientific. Fluorescence dye Alexa Fluor 594 cadaverine (AF594) and Lambda-Exonuclease (λ-Exo) were purchased from Life Technologies. Dimethyl sulfoxide (DMSO), used as the solvent for the diluted stock solution of AF594, was purchased from Life Technologies. While 1x PBS (Phosphate buffered saline) buffer was purchased from Corning Life Sciences.

The main chemical formulas in this research are listed in the Table 3.1.

Table 3.1. chemical formulas of PMMA, EDC, NHS and AF594

PMMA	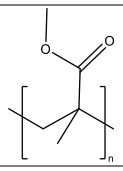
EDC	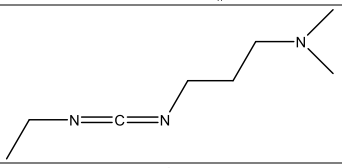
NHS	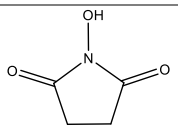
APTES	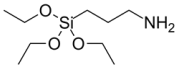
AF594**[85]**	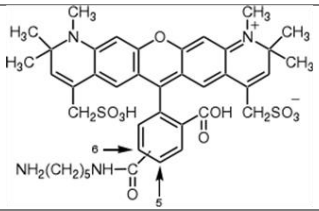

3.2. Surface treatment

3.2.1. O_2 plasma treatment

O_2 plasma treatment was performed through RIE (Technics Micro-RIE 800 series). Based on the previous works from our group, the treatment condition to expose PMMA to O_2 plasma was determined to be 30s, 50W. Which can obtain a well balance between high density of functional groups and severe damage on the surface morphology. The equipment for O_2 plasma treatment and the vacuum chamber is shown in figure 3.1 (a).

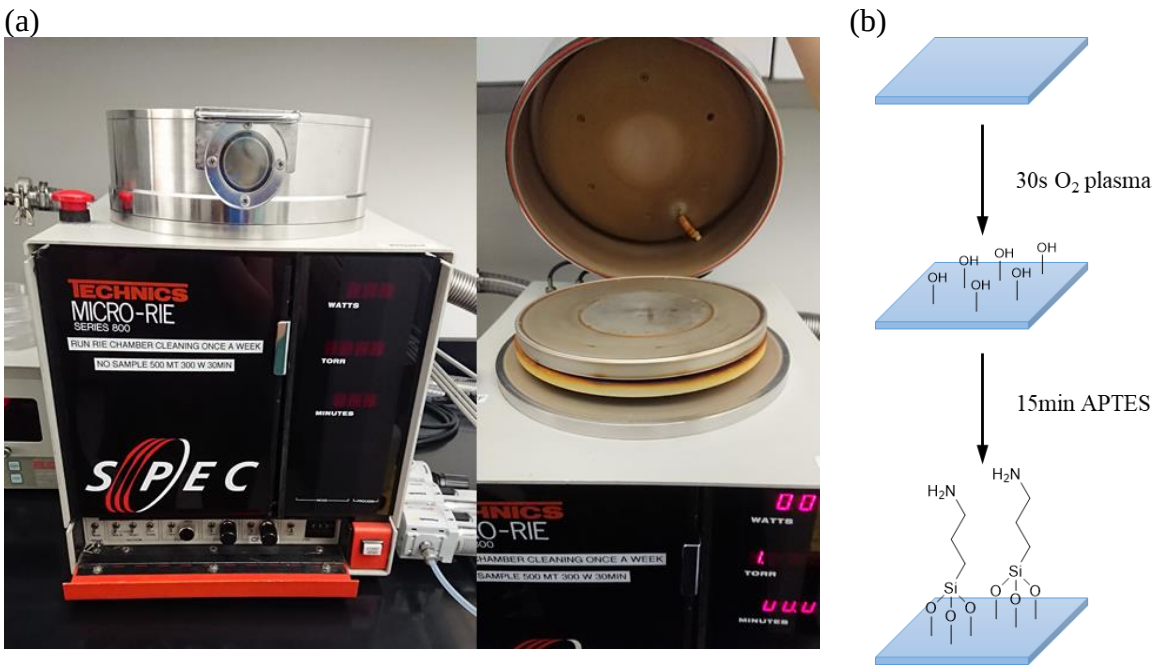

Figure 3.1. (a) RIE equipment and its cylindrical vacuum chamber; (b) reaction process of APTES bond PMMA.

After 30s O_2 plasma treatment, PMMA was incubate in APTES solution for 15min at room temperature. APTES molecules react with hydroxyl groups generated during O_2 plasma treatment and form aminopropylsilane (APS) film on PMMA with the amino terminal ends as shown in figure 3.1(b). The PMMA with -NH_2 terminals was measured zeta potential to offer additional information.

3.2.2. UV/O_3 treatment

In this research, UV/O_3 treatment was achieved by a homemade UV/O_3 radiation machine(254 nm,16 mW/cm^2), as figure 3.2 shows. PMMA samples were set inside the chamber during irradiation and Al foil was used to cover the gaps of the chamber to protect people from leakage of O_3. For the same reason, this machine must be run inside a hood with good air circulation. The time of treatment was measured manually. In this research, the exposure time of UV/O_3 were 1 minute, 5 minutes and 15 minutes, respectively.

Figure 3.2. Homemade UV/O_3 irradiation machine with Al foil covered.

3.2.3. EDC/NHS functionalization

O_2 plasma or UV/O_3 treated PMMA would take EDC/NHS functionalization by immersing PMMA in a solution containing 200 mM EDC and 50 mM NHS in 0.1 M MES at room temperature. The incubation time are 15min, 30min and 1h separately. Because of the instability of EDC and NHS, the incubation process is performed in dark, and the EDC/NHS solution should be used immediately after preparation and must be stored at 4℃ without light. After incubation, PMMA samples were washed with DI water and dry with N_2 gas gently.

3.2.4. Binding of fluorescent dye on PMMA surface

In this research, AF594 was selectively immobilized onto UV/O_3 treated PMMA surfaces using EDC/NHS coupling chemistry. To be specific, PMMA was covered by a photomask

during UV/O_3 treatment, which was consisted by silicon substance and patterned Cr surface. There were two kinds of pattern on the photomask, strips and dots, as shown in figure 3.3.

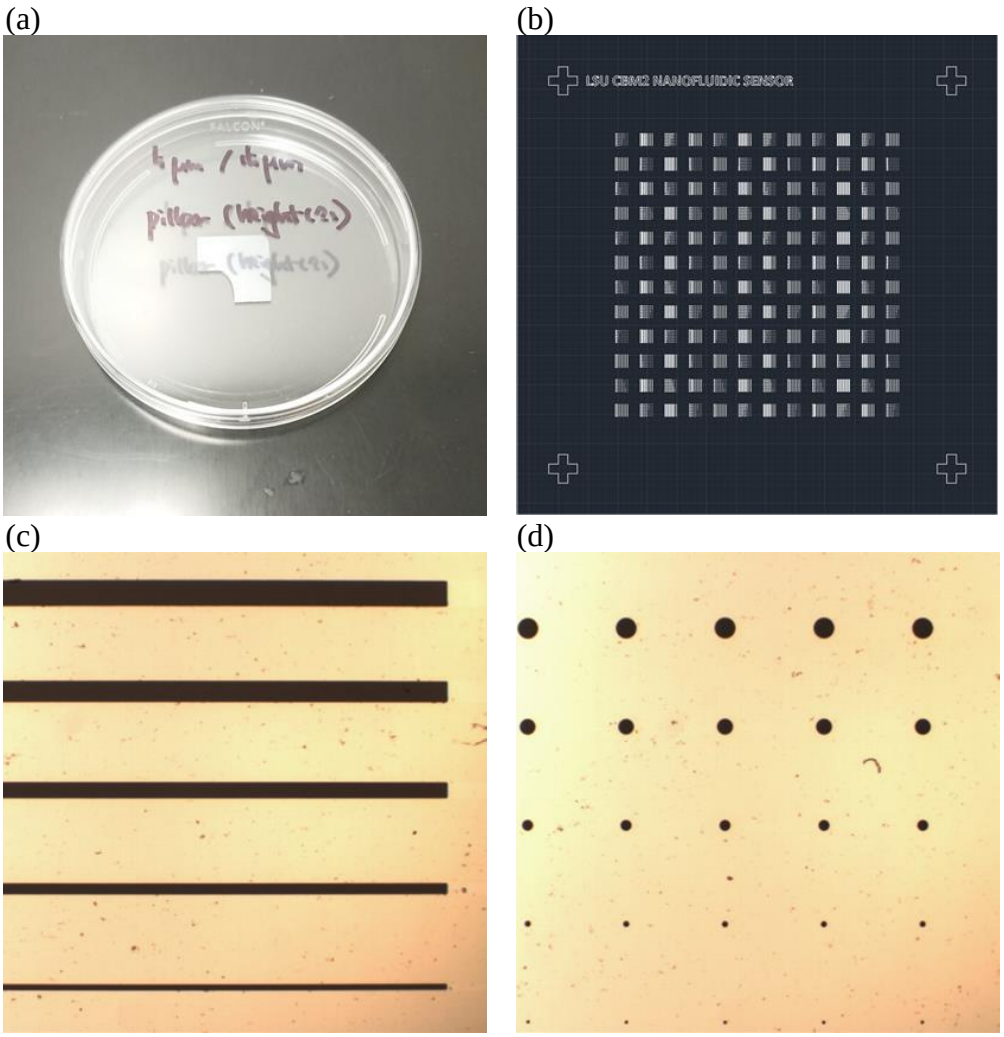

Figure 3.3. (a) picture of the photomask; (b) the drawing file of the photomask; (c, d) two patterns observed under ordinary microscope.

After UV/O_3 irradiation, PMMA was incubated in EDC/NHS solution for 30 minutes then washed with DI water. After gently drying the sample surface by gas, PMMA was immersed by the solution containing 0.05mM AF594 in MES and incubated in dark at room temperature for 1 hour. Then PMMA was washed with DI water and dried thoroughly before observation under fluorescence microscope.

3.2.5. Binding of lambda-exonuclease on PMMA surface

The enzyme anchored onto PMMA was chosen to be Lambda-Exonuclease (λ-Exo). In this experiment, λ-Exo was introduced onto the PMMA surfaces after 1-minute UV/O_3 and 30-minute EDC/NHS activation. The samples covered by the solution containing λ-Exo were incubated for 2 h at room temperature. Then devices were washed with 1x PBS to remove unbound enzyme or other chemicals and subsequently stored at 4°C until use. The concentration of λ-Exo solution is 0.2 U/μl, 0.4 U/μl and 0.8 U/μl separately.

Before immobilization treatment of λ-Exo onto PMMA, the storage buffer of the enzyme must be exchanged with 1x PBS. Because the storage buffer the enzyme was supplied in contained 25 mM Tris-HCl, which will interfere with the covalent attachment due to a primary amine group in Tris. The buffer exchange process was completed via 0.5ml Zeba Spin Desalting Columns, 7K MWCO (Pierce Biotechnology), and the detailed steps were described in the instruction.

The whole procedure of this experiment is shown in figure 3.4.

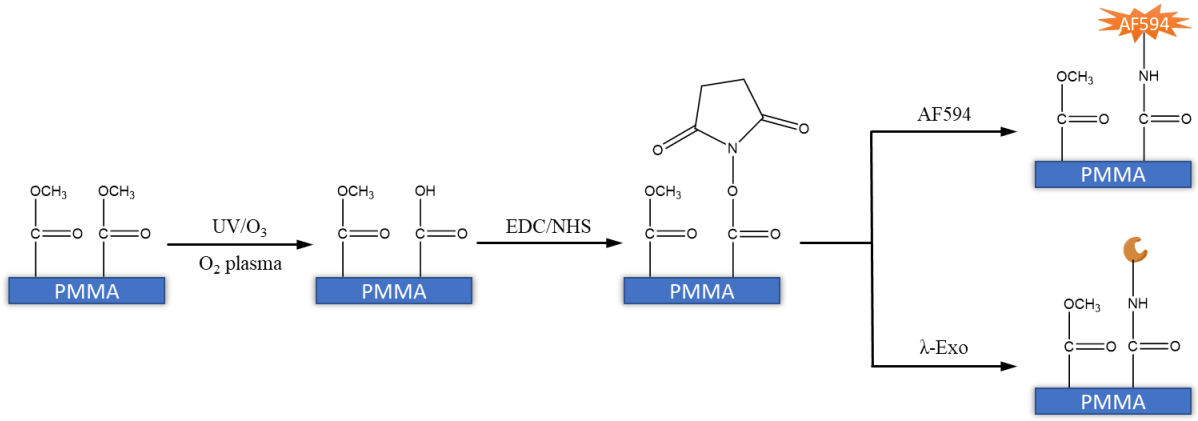

Figure 3.4. the scheme of the experimental processes.

3.3. Characterization

3.3.1. Zeta potential measurements

The zeta potential measurement of PMMA samples was performed by SurPASS 3 (Anton Paar). To calculate the zeta potential of flat substrates, two pieces of samples with the area in proximity of $10mm \times 20mm$ were mounted on parallel stages in the measurement cell of SurPASS 3 (figure 3.6(b)). After fixing the measurement cell on the system, the gap between two samples was manually adjusted to $100\mu m$ during rinsing steps.

(a) (b)

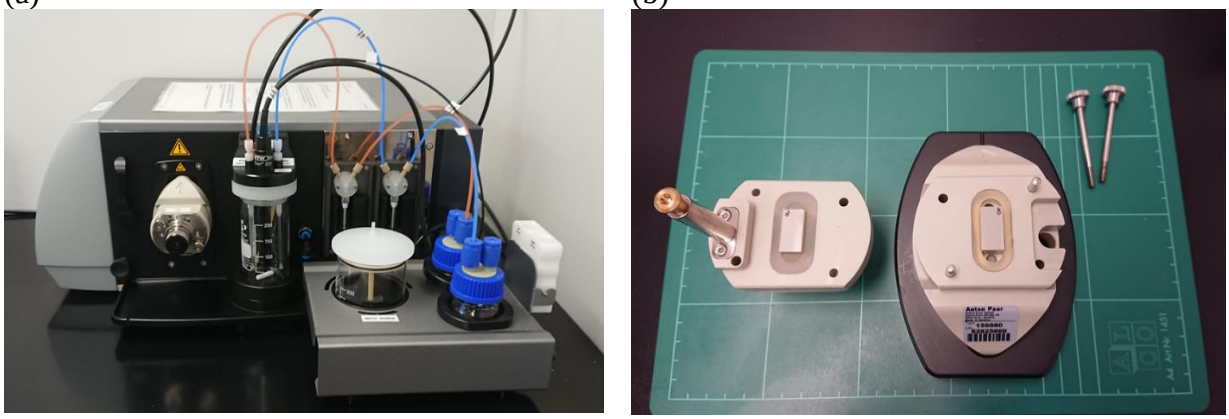

Figure3.5. (a) the picture of SurPASS 3 from Anton Paar; (b) the measurement cell of SurPASS 3 with PMMA mounted.

As a flow of aqueous electrolyte solution, which was 0.001M KCl solution, was supplied through the gap between two samples in a controlled pressure system, the values of the streaming potential and streaming current were automatically measured by SurPASS 3 and the zeta potential of materials surface was calculated based on the equation:

$$I_{str} = \frac{\Delta P \epsilon_r \epsilon_0 \zeta A}{\eta L} \qquad (3.1)$$

The zeta potential measurements were performed on at least three groups of PMMA with a same condition to obtain an average value. The electrokinetic surface charge density of the

sample was converted from the average value of the zeta potential based on the Grahame equation:

$$\sigma_\zeta = \frac{2\epsilon_r \epsilon_0 k_B T}{e\lambda_D} \sinh\left(\frac{e\zeta}{2k_B T}\right) \qquad (3.2)$$

3.3.2. Water contact angle measurements

Surface roughness and surface energy has strong effects on the wettability of surface; therefore, water contact angle measurements were performed as additional proofs to reveal the influence of surface treatments. The water contact angle of PMMA with the deposited droplet of 5 μL distilled water was pictured and roughly measured by ImageJ software.

3.3.3. Fluorescence microscopy

In order to check the effectiveness of EDC/NHS treatment, PMMA samples were observed by fluorescence microscope (Olympus IX70) and fluorescence imaging was performed by a CCD camera (Photon Max, Princeton Instruments). The observation was conducted in the dark to reduce the interfere of environmental lights on fluorescence signals.

Except PMMA substances with selectively labelling, control samples were also prepared and observed to exclude non-specific fluorescent signals. The control samples were UV/O_3 and EDC/NHS activated PMMA with totally same conditions and without any AF594 treatment.

Both experimental samples and control samples were observed under the microscope with the same camera settings.

Chapter 4. Zeta potential of PMMA after surface activation

4.1. Introduction

Nanofluidic is impacted significantly by several unique phenomena: electric double layer, ion-current rectification, surface charge and entropic barriers. Thus, designing a nanofluidic device must take the electrokinetic forces of materials into consideration. Polymeric materials are attractive alternatives for commercial silicon or glass in nanofabrication.

Due to the natural hydrophobicity and less reactive functional groups on polymers,[8] utilizing polymer in nanofluidic devices requires proper surface activation techniques. UV/O_3 and plasma treatment are common methods to functionalize polymer surface, alter the wettability behavior, and increase adhesion between different substance. And the evaluation of the effectiveness of surface modification methods is an essential step.

Because zeta potential reflects the electrical potential at the shear plane of the electric double layer of a material, the measurement of zeta potential can be a characterization method to estimate the surface charge and help in optimizing the fabrication route of polymeric nanofluidic systems.

In this chapter, the thermoplastic, PMMA was activated by UV/O_3 and O_2 plasma treatments separately, and was measured its zeta potential value. The results will indicate the consequences of surface functionalization.

4.2. Zeta potential of PMMA upon O_2 plasma treatment

O_2 plasma are common techniques to modify polymer surface. The zeta potential measurement results with 0.001M KCl concentrations and electrokinetic surface charge density of PMMA as a function of pH value were provided in figure 4.1. Three plots explicate the

difference of zeta potentials among untreated PMMA, O_2 treated PMMA and APTES anchored PMMA at a pH range of 2.5-10.

(a) (b)

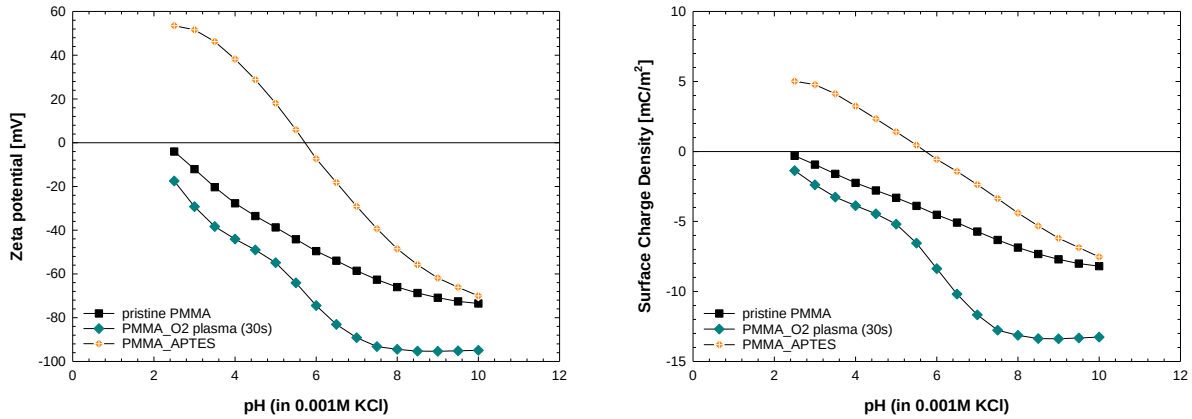

Figure 4.1. Plots of (a) zeta potential measurements of PMMA; (b) surface charge density of PMMA. Black line represents the value of untreated PMMA, green line represents the value of PMMA after 30s O_2 plasma treatment and orange line represents PMMA taken 30s O_2 plasma treatment followed by 15min 3-APTES incubation.

The overall trend of three lines is decreasing with increased pH value for all three conditions. This phenomena can be explained by deprotonation. At low pH, hydrophilic sites on PMMA surface tends to adsorb protons due to the high proton concentration, which leads to a relatively less negative electrokinetic surface charge density. On the contrary, the surface is more negative charged at high pH.

Initially, the zeta potential of PMMA at pH 10 is -75mV and end at -17mV at pH 2.5. After 30s O_2 plasma treatment, the zeta potential is decreased 10-20mV over all the pH. The decrease in the zeta potential after O2 plasma treatment can be explained by the relationships between zeta potential and the surface properties. O_2 plasma treatment introduces functional groups containing oxygen into polymer surface. For PMMA, the dominate functional group is carboxylic acid, -COOH, which leads to more negatively charged surface.[46]

Another finding about O_2 plasma treated PMMA is that the slope of zeta potential vs. pH curve changes with different pH. At pH < 7, the decrease of zeta potential was steeper than that at pH > 7. This phenomenon should attribute to the dissociation of carboxyl groups:

$$COOH \leftrightharpoons COO^- + H^+ \quad (4.1)$$

At low pH, many carboxyl groups remained in uncharged, and when pH increased, the ionized state $-COO^-$ increased, resulting in the negative increase in the zeta potential.

It is obvious that the zeta potential of APTES treated PMMA is highest. And the difference is more significant at lower pH value. This plot confirms the generation of carboxyl on PMMA after O2 plasma treatment by clarifying the existence of -NH_2. As mentioned in Ch 3.2.1, APTES molecules react with hydroxyl groups via condensation reaction and form APS film on PMMA with the amino groups in contact with the electrolyte solution. And the reason behind the increased zeta potential is the ionization of the amino:

$$NH_3^+ \leftrightharpoons NH_2 + H^+ \quad (4.2)$$

Therefore, APTES treated PMMA shows most positive surface charge and the highest IEP among three samples.

4.3. Zeta potential of PMMA upon UV/O_3 treatment

Figure 4.2 (a) is the zeta potential of PMMA exposed to UV/O_3 treated for 1 minutes, 5 minutes and 15 minutes respectively. Since carboxylic acid functional groups also dominate on the PMMA surface after UV/O_3 irradiation, there is supposed to be a similar trend in the plots of UV/O_3 treated PMMA comparing with the zeta potential of O_2 treated PMMA. However, though 1min UV/O_3 treated PMMA (PMMA_1min UVO) looks similar to O_2 plasma treated PMMA, other two plots of zeta potentials of PMMA with longer treatment time have distinct trends.

As shown in figure 4.2 (a), the value of PMMA after 5min UV/O_3 treatment (PMMA_5min UVO) is close to that of pristine PMMA at pH 10, and then it keeps decreasing at pH 7-9 until it reaches to the lowest point at pH 6.5. For PMMA after 15min UV/O_3 treatment (PMMA_15min UVO), its absolute value of zeta potential is even lower than pristine PMMA in the pH range of 6-10.

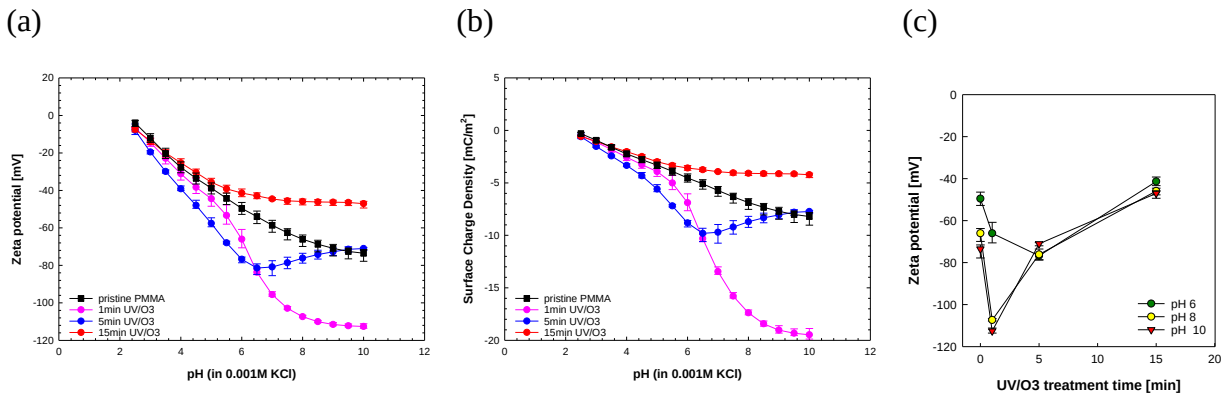

Figure 4.2. Plots of PMMA after UV/O_3 treatment: (a) zeta potentials of PMMA and (b) surface charge density as a function of pH value with the comparison of untreated PMMA. UV/O_3 treatment time are 1min, 5min and 15min, represented in pink, blue and red respectively; (c) zeta potential of PMMA as a function of UV/O_3 treatment time. Green line represents the zeta potential measured at pH 6, blue for pH 8 and red for pH 10 respectively.

Figure 4.2 (c) presents the zeta potential of PMMA as a function of UV/O_3 treatment time at pH 6, 8 and 10. The three pH values were selected because they are suitable for biological applications. More specifically, solution in pH 6 is mild to maintain activities and stabilities of many proteins, whilst pH 8 and pH 10 are applied in our group for biomolecules translocation inside nanofluidic devices.

It can be concluded that with increasing exposure time of UV/O_3 treatment, PMMA takes a dramatic decrease in the negative electrokinetic surface charge. This apparent decrease can be partially explained by the negative influence of long-time exposure on−COOH density. Along with the generation of carboxylic acid on the surface, the radical reactions occurs, and reactions as $-CO_2$ release, scission of the polymer chain, and etching of the surface can degrade the

−COOH group and lead to a lower surface charge density[46]. However, for PMMA_15min UVO, its lowest absolute value of zeta potential may suggest a significant degradation of surface functional groups.

The zeta potential values and electrokinetic surface charge densities of PMMA with different modifications are summarized in Table 4.1.

Table 4.1. Zeta potential and electrokinetic surface charge density of PMMA at pH 6.0, 8.0 and 10.0**.**

PMMA		pH 6.0	pH 8.0	pH 10.0
Pristine	$\zeta\ [mV]$	-48.51 ± 2.47	-64.74 ± 1.51	-72.09 ± 0.46
	$\sigma\ [mC/m^2]$	-4.39 ± 0.29	-6.62 ± 0.22	-7.92 ± 0.08
30 s O_2 plasma	$\zeta\ [mV]$	-74.46 ± 2.24	-94.49 ± 2.17	-94.92 ± 2.29
	$\sigma\ [mC/m^2]$	-8.37 ± 0.43	-13.13 ± 0.65	-13.32 ± 0.64
1 min UV/O_3	$\zeta\ [mV]$	-66.06 ± 4.93	-107.36 ± 0.65	-112.58 ± 1.27
	$\sigma\ [mC/m^2]$	-6.89 ± 0.81	-17.39 ± 0.23	-19.47 ± 0.51
5 min UV/O_3	$\zeta\ [mV]$	-76.74 ± 3.00	-76.14 ± 2.64	-71.03 ± 0.84
	$\sigma\ [mC/m^2]$	-8.82 ± 0.31	-8.70 ± 0.53	-7.72 ± 0.14
15 min UV/O_3	$\zeta\ [mV]$	-74.46 ± 2.24	-94.49 ± 2.27	-94.92 ± 2.29
	$\sigma\ [mC/m^2]$	-8.37 ± 0.43	-13.13 ± 0.65	-13.26 ± 0.65

4.4. The effect of scan direction for UV/O_3 treated PMMA

To figure out the reason behind the abnormal low surface charge density, additional zeta potential measurement was conducted. The zeta potential of PMMA was usually measured continuously from high pH to low pH, but in this section, the measurement circle started from pH 6 to pH 10. Then measured the same PMMA sample in opposite direction of pH from 10-6, marked as second scan. Finally, PMMA was measured again from pH 6-10, called third scan.

The three times of measurements were performed on PMMA after 30s O_2 plasma and 15min UV/O_3 respectively.

(a) (b)

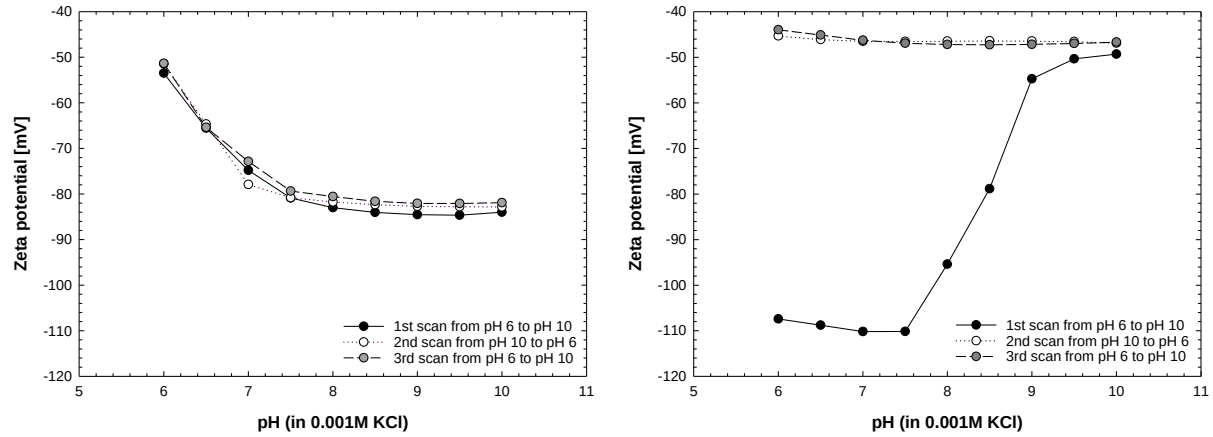

Figure 4.3. three times of zeta potential measurement on two PMMA treated by (a) 30 seconds O2 plasma; (b) 15 minutes UV/O3 respectively. Black. white and gray curves represent the first, second and third time of measurement scan separately.

As figure 4.3 shows, for O_2 plasma treated PMMA, the zeta potential values of three measurement circles are almost overlapped. The curves in figure 4.3 (a) indicate reliable measurement results and stable functionalized PMMA surface. On the contrary, the first scan of PMMA_15min UVO is completely different from other two scans. Initially, the zeta potential value of PMMA_15min UVO at pH 6 is -108 mV, 40mV lower than pure PMMA and 20mV lower than PMMA_1min UVO. The zeta potential value remains low at pH 6-7 but dramatically and steeply increases as the pH of electrolyte solution over 8. Finally, the zeta potential of this sample remains in the range of -40~-50mV no matter how pH changes. This value also agrees with the measurement results of PMMA_15min UVO in the last section.

It is natural to assume that PMMA_15min UVO is degraded in the contact with the alkaline solution. To be specific, the PMMA polymer is exposed to a highly oxidative atmosphere and irradiation by high-energy photons during UV/O_3 treatment, which partly

oxidized the polymer chains as well as fragmented the surface groups. Some low molecular weight oxidized material could not vaporize easily and remained on the surface. When these fragments are subjected to washing during the zeta potential measurements, they could be lost by dissolution and lead to a decreased surface charge density. The removal of the functionalized surface after UV/O_3 irradiation was also reported to occur in commercial multi-electrode array (MEA), polymers like COC, PET and PMMA,[56, 86–88] where the changes in thickness, surface atom and water contact angle were included.

4.5. Water contact angle measurements

Since the degradation of PMMA surface can impact the water contact angle. The water contact angle of multiple PMMA substances were roughly measured. Table 4.2 lists the surface pictures of pure, O_2 plasma treated PMMA and PMMA_15min UVO with their corresponding water contact angles.

Table 4.2. surface of PMMA substances and their water contact angle before and after zeta potential measurement.

	Pristine PMMA	PMMA_30s O_2 plasma	PMMA_15min UVO
Before zeta potential measurement	 ∠68°	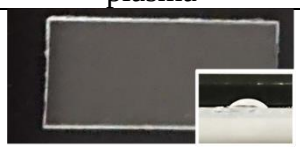 ∠44°	 ∠45°
After zeta potential measurement	 ∠63°	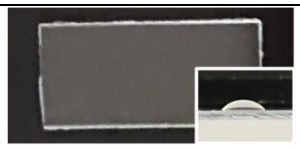 ∠42°	 ∠70°

As shown in table 4.2. the wettability of pristine PMMA is not good. After activation of O_2 plasma or UV/O_3, the water contact angle decease from 70° to 40° immediately. hydrophilic surface. The decrease in water contact angle agrees with other observation results for the reason that two activation methods increase surface energy. And the interesting result is that after zeta

potential measurement process, the water contact angle does not change for PMMA_30s O_2 plasma but significantly increases to 70° for PMMA_15min UVO. After contacting with electrolyte in the pH range of 2-10, PMMA_15min UVO not only lost the hydrophilicity but also lost its transparency.

The decrease of hydrophilicity and transparency agrees with the assumption that fragments on PMMA_15min UVO are dissolved in solution. As a result, surface energy drops with the reduction of the amount of carboxyl, while the surface topography changes.[87]

More images of PMMA surface as a function of UV/O_3 irradiation time are listed in Table 4.3. It is obvious that for short exposure time such as 1min, the change of wettability and transparency is not evident. As the exposure time rises above 5min, the wettability becomes better. But after immersing in KCl solution during characterization, the wettability of all four samples is similar with the water contact angle of 70°.

Table 4.3. surface of PMMA substances and their water contact angle before and after zeta potential measurement.

Before zeta potential measurement				
After zeta potential measurement				

Chapter 5. EDC/NHS Functionalization of PMMA

5.1. Introduction

EDC/NHS coupling chemistry is commonly used to conjugate biological substances containing carboxylates and amines. EDC is a zero-length crosslinker, which reacts with a carboxylate group to form an *O*-acylisourea active ester. The intermediate is then replaced by NHS ester groups which ultimately reacts with the amine-containing molecule. Finally, covalent bond between carboxylates and amines is formed without additional spacing or atom.

Proper polymer-based nanofluidic devices is able to anchor diverse proteins via EDC/NHS coupling chemistry to adjust properties such as surface charge, permeability flux or biocompatibility.

In this paper, EDC/NHS functionalization is also necessary to immobilized enzyme onto PMMA substance. The zeta potential of PMMA after EDC/NHS treatment was measured in this chapter to evaluate the difference in surface charge among samples with three treatment time. The effectiveness of EDC/NHS was also confirmed via fluorescence labelling of a amine-containing dye.

5.2. EDC/NHS Functionalization on O_2 plasma and UV/O_3 treated PMMA

EDC/NHS coupling chemistry is used on PMMA surface after UV/O_3 or O_2 plasma treatment. The O_2 plasma treatment is 30s exposure, but UV/O_3 irradiation condition is uncertain. 1-minute UV/O_3 irradiation is preferred based on the measurement results as mentioned in chapter 4, where PMMA_1min UVO possesses lowest surface charge density which may indicating largest amount of -COOH. However, other researchers prefer 15-minute UV/O_3 irradiation for their PMMA devices.[11, 70, 89]

To determine the best time of UV/O_3 irradiation in this experiment, EDC/NHS treatment was performed on PMMA after 1 minute and 15 minutes UV/O_3 respectively. The comparison of the zeta potential of PMMA with two UV/O_3 treatments before and after 15 minutes EDC/NHS treatment is provided in figure 5.1.

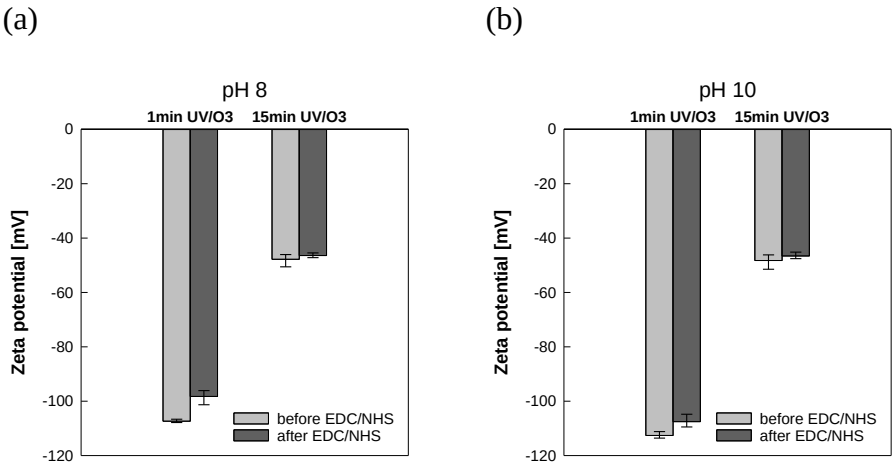

Figure 5.1. Box plot of zeta potential of PMMA before and after 15 minutes EDC/NHS functionalization with 1min and 15min UV/O_3 treatment at (a) pH 8; (b) at pH 10.

From figure 5.1., PMMA_1min UVO tends to obtain higher density of negative surface charge compared with PMMA_15min UVO. The relatively larger gap of zeta potential between PMMA_1min UVO before and after EDC/NHS treatment suggests that it has more carboxylic acid on the polymer surface to react with EDC/NHS reagent, since -COOH is ionic at high pH while NHS or EDC intermediate is neutral. Thus, 1min UV/O_3 is determined and the optimal EDC/NHS treatment condition is going to be decided.

Three conditions: 15-minute, 30-minute and 1-hour incubation of EDC/NHS solution were executed on PMMA after 1min UV/O_3 irradiation and 30s O_2 plasma treatment. Figure 5.2. shows their values of zeta potential and surface charge densities in the pH range of 2-10 in 0.001M KCl solution.

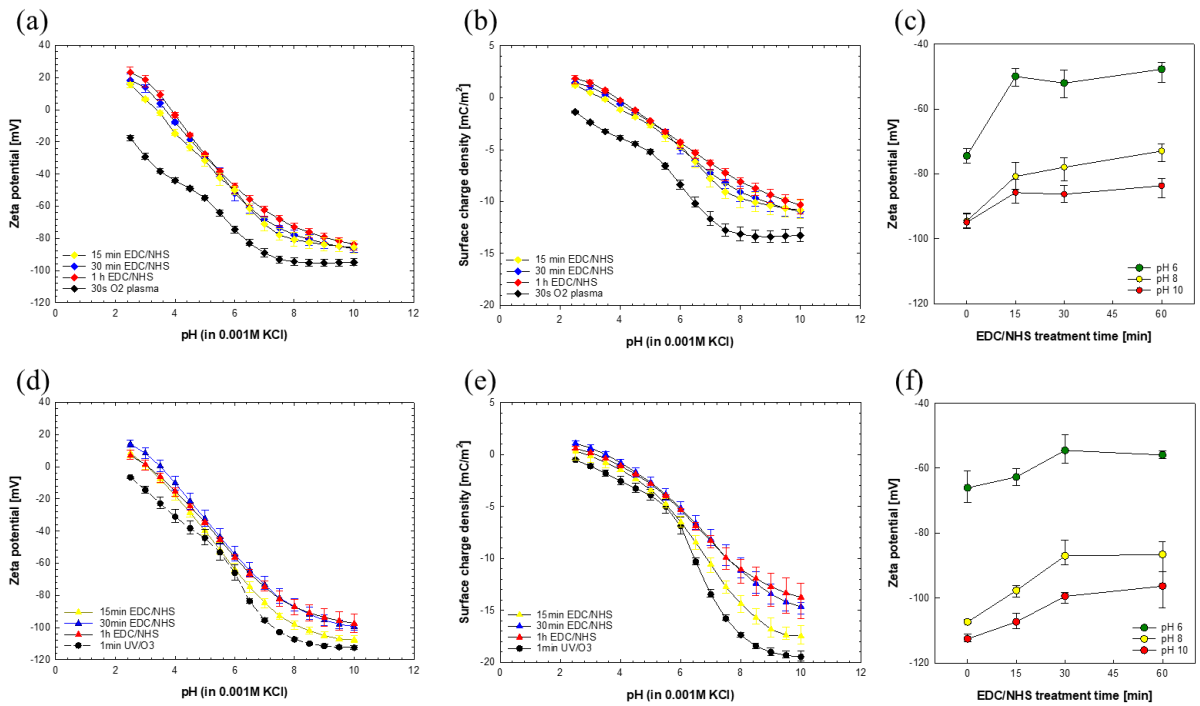

Figure 5.2. PMMA treated by three EDC/NHS treatment conditions after (a-c) 30s O_2 plasma treatment; (d-f) 1min UV/O_3 irradiation. Where (a, d) are plots of zeta potential values, (b, e) are plots of electrokinetic surface charge density and (c, f) are zeta potential of PMMA as a function of EDC/NHS treatment time.

Overall, the zeta potential measured on all three kinds of EDC/NHS functionalized samples are similar with lower absolute value than that of PMMA after O_2 plasma and UV/O_3 treatment, respectively. The increased zeta potential indicates the reduction of carboxyl, which agrees with the shift of isoelectric point (IEP) for O_2 plasma and UV/O_3 activated PMMA. IEP is the pH value at which samples exhibit zero zeta potential. For PMMA before EDC/NHS treatment, IEP is lower than 2. After EDC/NHS treatment, IEP increases to 3-4 suggesting that the EDC or NHS reagents were anchored to carboxylic acid groups on PMMA.

Figure 5.2 (c) reveals the similarity of zeta potentials on O_2 plasma treated PMMA with three EDC/NHS treatment conditions. On the other hand, UV/O_3 activated PMMA shows divergence where 30min and 1h EDC/NHS treated PMMA have similar high zeta potentials, and 15min EDC/NHS treated PMMA has relatively low zeta potentials.

For figure 5.2 (a), it is noticeable that at low pH, the difference of O_2 plasma treated PMMA with and without EDC/NHS treatment increases evidently than its counterpart shown in figure 5.2 (d). This may indicate a relatively more sufficient functionalization on PMMA after O_2 plasma activation. Besides, this result may attribute to the greater hydrophilicity of PMMA with the improved attraction to proton.

5.3. Binding of a fluorescein on EDC/NHS functionalized PMMA

It has to be acknowledged that the EDC/NHS treatment did not introduce a significant reduction in surface charge of UV/O_3 treated PMMA. The potential explanations include inadequate physical activation, instability of the EDC and NHS chemicals.

To verify the effectiveness of EDC/NHS functionalization on PMMA, UV/O_3 treated PMMA was labelled by a red-fluorescent dye, AF594, via covalent attachment. During UV/O_3 irradiation, a photomask was applied to generate patterns on PMMA via generation of carboxyl groups on selected area.

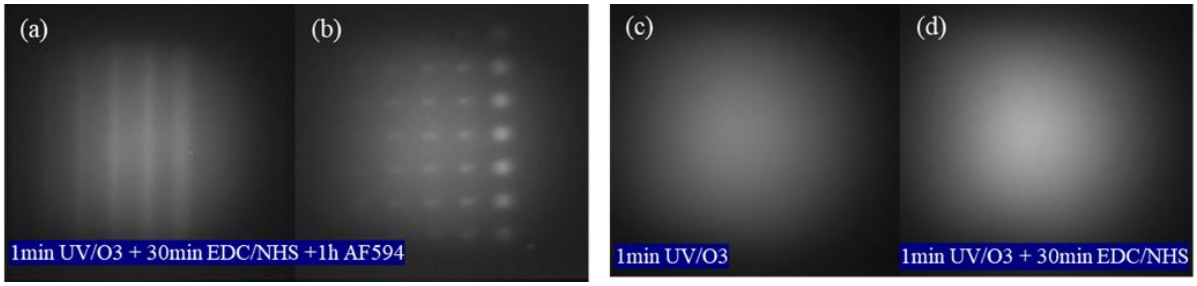

Figure 5.3. (a, b) images of the two patterns on AF594 labelled PMMA which was activated selectively under fluorescence microscope; (c) fluorescence images of PMMA with UV/O_3; (d) fluorescence images of PMMA with UV/O_3 and EDC/NHS.

Figure 5.3 (a, b) reveals the two patterns observed under the fluorescent microscope, implying the successful attachment of fluorescent dye to PMMA. To exclude potential non-specific signal, control samples were prepared and observed under the same fluorescence microscope. Without incubation of AF594, no pattern is found as shown in figure 5.3 (c, d).

Which excludes the possibility that the patterns occur due to other causes such as ozone and adsorbed dye.

Chapter 6. Immobilization of Enzyme

6.1. Introduction

Realizing biological reactions via the integration of enzymes in nanofluidic systems expands the range of applications of nanofluidic devices. Immobilized enzyme on polymeric devices can enhance reaction efficiency and increase system automation.[75] For example, lambda-exonuclease (λ-Exo) immobilized IMER will clip DNA into nucleotides automatically. Coupled by an appropriate detection method, this device is capable of DNA sequencing without additional treatments such as DNA labeling.

Immobilizing enzyme on PMMA has been reported,[70] but the direct data of the change in surface charge of PMMA after protein immobilization is limited. The binding affinities of proteins and carrier particles in the relation with their experimental measured value of zeta potential was studied by Schultz et al.[90] Similarly, in previous chapters, zeta potential measurement was utilized to guide an optimal condition for surface modification. Here, the λ-Exo attached PMMA is characterized by zeta potential measurement to evaluate the efficiency of the immobilization method.

6.2. Zeta potential on immobilization of *λ*-Exo

Based on the conclusion from chapter 4 and chapter 5, 1-minute UV/O_3 and 30-minute EDC/NHS treatment were taken by PMMA prior to the enzyme immobilization. This condition is determined based on the results from previous section to maximize the activated surface functional groups. While O_2 plasma treatment was omitted considering the more negative charged surface of UV/O_3 treated PMMA.

λ-Exo solution in three concentration, 0.2U/μl, 0.4U/μl, 0.8U/μl was used in immobilization step. Figure 6.1 show the zeta potential and surface charge density of three

groups of PMMA. Since the EDC/NHS ester will be replaced during the formation of the covalent bonding between -COOH on PMMA and -NH_2 on λ-Exo, figure 6.1 exclude the zeta potential of PMMA after EDC/NHS treatment.

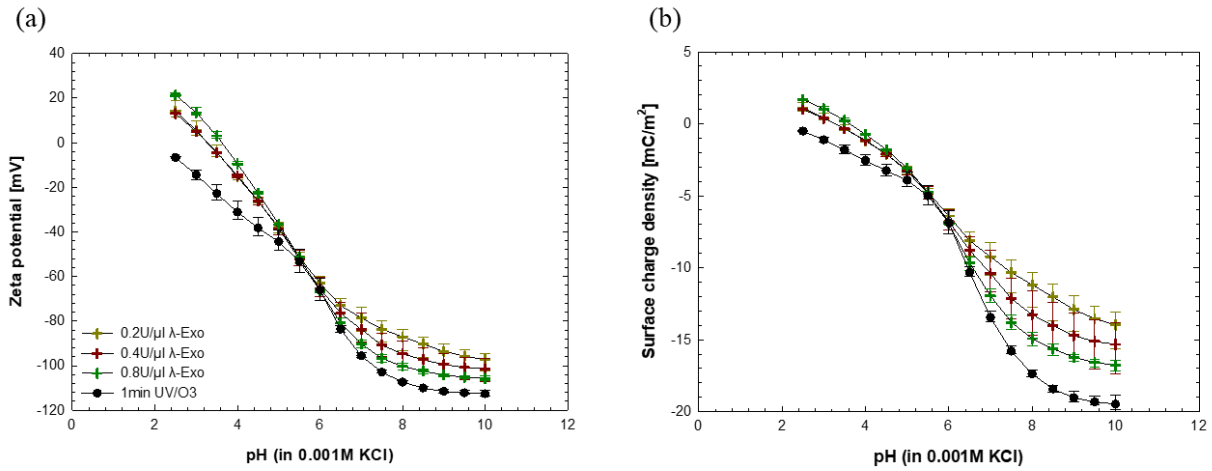

Figure 6.1. plots of PMMA incubated in λ-Exo solution as a function of pH value: (a) zeta potential; (b) surface charge density. Where yellow line represents PMMA taken 0.2U/µl λ-Exo solution, black and green lines represent that of 0.4U/µl and 0.8 U/µl λ-Exo solution, respectively.

As figure 6.1 shows, three groups of PMMA after enzyme immobilization all have lower absolute value of zeta potential as well as higher IEP compared with PMMA_1min UVO, which confirms the reduction of carboxylic acid and implies the anchoring of λ-Exo.

There is apparent separation in zeta potential among three kinds PMMA at pH from 6 to 10. The group taken 0.2U/µl λ-Exo (PMMA_0.2U/µl λ-Exo) solution had the smallest absolute value of zeta potential as well as minimum surface charge density, whereas group with 0.8U/µl λ-Exo solution (PMMA_0.8U/µl λ-Exo) had the largest absolute value of zeta potential and maximum surface charge density. However, the IEP of PMMA_0.2U/µl λ-Exo is smaller than that of PMMA_0.8U/µl λ-Exo. The reverse of the position of λ-Exo immobilized PMMA might attribute to the nature of proteins that is, surface charge of an enzyme depends on pH and

temperature. During measurement circle, the temperature was constant, but pH value varied. At high pH, λ-Exo tends to be negative charged while it turns to be positive at low pH. Herein, the two plots may reveal that the PMMA has larger amount of enzyme anchored to when immersed in λ-Exo solution with higher concentration. Still, because the three PMMA groups are close to each other, this conclusion is not very convincing.

Chapter 7. Conclusions and Future Work

7.1. Conclusions

In this research, we investigated zeta potential and electrokinetic surface charge density for PMMA after various surface modification methods, including UV/O_3 irradiation and O_2 plasma activation, EDC/NHS functionalization and enzyme immobilization.

Corresponding to each modification way, the absolute values of zeta potential as well as the surface charge density of PMMA fluctuated. The fluctuation indicated the changes of surface functional groups on PMMA. For UV/O_3 treated PMMA, the absolute value of zeta potential was increased since the oxidation of surface functional groups offers ionic species, carboxylic acid. And for EDC/NHS treatment and the following λ-Exo immobilization, the decreased absolute value of zeta potential suggested the bond between carboxyl and reactive EDC/NHS reagent or amine-containing molecules separately.

The zeta potential measurement results reflect the electrokinetic surface charge density of PMMA, which shows the potential of this characterization method in directing experiment conditions. Considering the simple and easy-handled measurement process, zeta potential measurement can also be applied in other polymeric materials to maximum outcomes in an efficient way.

7.2. Future work

This research can be developed further by adding modification conditions. For example, the incubation time of λ-Exo in three concentration can be extended to analyze the influence of long-time treatment of enzyme on the productivity of immobilization.

Moreover, the limitation of zeta potential measurement is inevitable. The measurement result is affected not only by surface charge but also by other factors, such as surface roughness,

temperature, and concentration of the electrolyte solution. Moreover, the explanation behind a reliable zeta potential value is not isolated, the value is the consequence of surface functional group, wettability, interaction with air or solvent, and other factors. It is difficult to justify surface properties of samples, especially for those having similar results. Thus, combining with other characterization techniques such as atomic force microscopy (AFM), X-ray photoelectron spectroscopy (XPS) or Fourier-transform infrared spectroscopy (FT-IR) is essential to build a comprehensive understanding on how the surface modification methods affect polymers.

Finally, enzyme immobilization is a promising technique for nanofluidic systems. Through the integration of diverse enzymes with enhanced activity and stability in nanofluidic devices, automotive real-time analysis of biomolecule is accessible. One significant future direction is to develop a stable polymer-based nanofluidic chip with active bioreactor and test the chip with plentiful biomolecules to establish a database for practical usage.

Reference

1. Haywood, D.G., Saha-Shah, A., Baker, L.A., Jacobson, S.C.: Fundamental Studies of Nanofluidics: Nanopores, Nanochannels, and Nanopipets. Anal. Chem. 87, 172–187 (2015). https://doi.org/10.1021/ac504180h
2. Harms, Z.D., Haywood, D.G., Kneller, A.R., Jacobson, S.C.: Conductivity-based detection techniques in nanofluidic devices. Analyst. 140, 4779–4791 (2015). https://doi.org/10.1039/C5AN00075K
3. Xue, L., Yamazaki, H., Ren, R., Wanunu, M., Ivanov, A.P., Edel, J.B.: Solid-state nanopore sensors. Nat. Rev. Mater. 5, 931–951 (2020). https://doi.org/10.1038/s41578-020-0229-6
4. Nanofluidics: A New Arena for Materials Science - Xu - 2018 - Advanced Materials - Wiley Online Library, https://onlinelibrary-wiley-com.libezp.lib.lsu.edu/doi/full/10.1002/adma.201702419
5. Venkatesan, B.M., Bashir, R.: Nanopore sensors for nucleic acid analysis. Nat Nanotechnol. 6, 615–624 (2011). https://doi.org/10.1038/nnano.2011.129
6. Jameson, J.L., Longo, D.L.: Precision Medicine — Personalized, Problematic, and Promising, http://www.nejm.org/doi/10.1056/NEJMsb1503104
7. Chantiwas, R., Park, S., Soper, S.A., Kim, B.C., Takayama, S., Sunkara, V., Hwang, H., Cho, Y.-K.: Flexible fabrication and applications of polymer nanochannels and nanoslits. Chem. Soc. Rev. 40, 3677–3702 (2011). https://doi.org/10.1039/C0CS00138D
8. Soper, S.A., Ford, S.M., Qi, S., McCarley, R.L., Kelly, K., Murphy, M.C.: Polymeric Micro- electr-o mechanical. 10
9. Pud, S., Chao, S.H., Belkin, M., Verschueren, D., Huijben, T., van Engelenburg, C., Dekker, C., Aksimentiev, A.: Mechanical Trapping of DNA in a Double-Nanopore System. Nano Lett. 16, 8021–8028 (2016). https://doi.org/10.1021/acs.nanolett.6b04642
10. Smeets, R.M.M., Keyser, U.F., Dekker, N.H., Dekker, C.: Noise in solid-state nanopores. Proc. Natl. Acad. Sci. 105, 417–421 (2008). https://doi.org/10.1073/pnas.0705349105
11. Athapattu, U.S., Amarasekara, C.A., Immel, J.R., Bloom, S., Barany, F., Nagel, A.C., Soper, S.A.: Solid-phase XRN1 reactions for RNA cleavage: application in single-molecule sequencing. Nucleic Acids Res. gkab001 (2021). https://doi.org/10.1093/nar/gkab001
12. Vashist, S.K.: Comparison of 1-Ethyl-3-(3-Dimethylaminopropyl) Carbodiimide Based Strategies to Crosslink Antibodies on Amine-Functionalized Platforms for Immunodiagnostic Applications. Diagnostics. 2, 23–33 (2012). https://doi.org/10.3390/diagnostics2030023
13. Peng, J., Su, Y., Chen, W., Zhao, X., Jiang, Z., Dong, Y., Zhang, Y., Liu, J., Xingzhong, C.: Polyamide nanofiltration membrane with high separation performance prepared by EDC/NHS mediated interfacial polymerization. J. Membr. Sci. 427, 92–100 (2013). https://doi.org/10.1016/j.memsci.2012.09.039
14. Prakash, S., Yeom, J.: Nanofluidics and microfluidics: systems and applications. William Andrew, Waltham (2014)
15. Bard, A.J., Faulkner, L.R.: Electrochemical methods: fundamentals and applications. Wiley, New York (2001)
16. Burgreen, D., Nakache, F.R.: Electrokinetic Flow in Ultrafine Capillary Slits [1]. J. Phys. Chem. 68, 1084–1091 (1964). https://doi.org/10.1021/j100787a019
17. Rice, C.L., Whitehead, R.: Electrokinetic Flow in a Narrow Cylindrical Capillary. J. Phys. Chem. 69, 8 (1965)

18. Yeh, L.-H., Xue, S., Joo, S.W., Qian, S., Hsu, J.-P.: Field Effect Control of Surface Charge Property and Electroosmotic Flow in Nanofluidics. J. Phys. Chem. C. 116, 4209–4216 (2012). https://doi.org/10.1021/jp211496b
19. Huang, C.-H., Lee, E.: Electrophoretic Motion of a Liquid Droplet in a Cylindrical Pore. J. Phys. Chem. C. 116, 15058–15067 (2012). https://doi.org/10.1021/jp301388a
20. Electrokinetic Transport in Nanochannels. 2. Experiments | Analytical Chemistry, https://pubs-acs-org.libezp.lib.lsu.edu/doi/10.1021/ac0508346
21. Hsu, J.-P., Yee, C.-P., Yeh, L.-H.: Importance of Electroosmotic Flow and Multiple Ionic Species on the Electrophoresis of a Rigid Sphere in a Charge-Regulated Zwitterionic Cylindrical Pore. Langmuir. 28, 10942–10947 (2012). https://doi.org/10.1021/la3018634
22. Chiu, Y.S., Keh, H.J.: Sedimentation velocity and potential in a concentrated suspension of charged soft spheres. Colloids Surf. Physicochem. Eng. Asp. 440, 185–196 (2014). https://doi.org/10.1016/j.colsurfa.2012.08.069
23. Keh, H.J., Liu, Y.C.: Sedimentation Velocity and Potential in a Dilute Suspension of Charged Composite Spheres. J. Colloid Interface Sci. 195, 169–191 (1997). https://doi.org/10.1006/jcis.1997.5147
24. Keh, H.J., Chen, W.C.: Sedimentation velocity and potential in concentrated suspensions of charged porous spheres. J. Colloid Interface Sci. 296, 710–720 (2006). https://doi.org/10.1016/j.jcis.2005.09.040
25. Das, S., Guha, A., Mitra, S.K.: Exploring new scaling regimes for streaming potential and electroviscous effects in a nanocapillary with overlapping Electric Double Layers. Anal. Chim. Acta. 804, 159–166 (2013). https://doi.org/10.1016/j.aca.2013.09.061
26. Bandopadhyay, A., Hossain, S.S., Chakraborty, S.: Ionic Size Dependent Electroviscous Effects in Ion-Selective Nanopores. Langmuir. 30, 7251–7258 (2014). https://doi.org/10.1021/la5014957
27. Chakraborty, J., Dey, R., Chakraborty, S.: Consistent accounting of steric effects for prediction of streaming potential in narrow confinements. Phys. Rev. E. 86, 061504 (2012). https://doi.org/10.1103/PhysRevE.86.061504
28. Sze, A., Erickson, D., Ren, L., Li, D.: Zeta-potential measurement using the Smoluchowski equation and the slope of the current–time relationship in electroosmotic flow. J. Colloid Interface Sci. 261, 402–410 (2003). https://doi.org/10.1016/S0021-9797(03)00142-5
29. Werner, C., Körber, H., Zimmermann, R., Dukhin, S., Jacobasch, H.-J.: Extended Electrokinetic Characterization of Flat Solid Surfaces. J. Colloid Interface Sci. 208, 329–346 (1998). https://doi.org/10.1006/jcis.1998.5787
30. Luxbacher, T.: The Zeta Potential for Solid Surface Analysis. Anton Paar GmbH. 136 (2014)
31. Jalil, A.H., Pyell, U.: Quantification of Zeta-Potential and Electrokinetic Surface Charge Density for Colloidal Silica Nanoparticles Dependent on Type and Concentration of the Counterion: Probing the Outer Helmholtz Plane. J. Phys. Chem. C. 122, 4437–4453 (2018). https://doi.org/10.1021/acs.jpcc.7b12525
32. Zhang, Y.N., Liu, X., Zhao, Y.A., Yu, J.K., Reisner, W., Dunbar, W.B.: Single Molecule DNA Resensing Using a Two-Pore Device. Small. 14, (2018). https://doi.org/10.1002/smll.201801890
33. Dekker, C.: Solid-state nanopores. Nat. Nanotechnol. 2, 209–215 (2007). https://doi.org/10.1038/nnano.2007.27

34. Storm, A.J., Chen, J.H., Ling, X.S., Zandbergen, H.W., Dekker, C.: Fabrication of solid-state nanopores with single-nanometre precision. Nat. Mater. 2, 537–540 (2003). https://doi.org/10.1038/nmat941
35. Karawdeniya, B.I., Bandara, Y.M.N.D.Y., Khan, A.I., Chen, W.T., Vu, H.-A., Morshed, A., Suh, J., Dutta, P., Kim, M.J.: Adeno-associated virus characterization for cargo discrimination through nanopore responsiveness. Nanoscale. 12, 23721–23731 (2020). https://doi.org/10.1039/D0NR05605G
36. Liu, X., Skanata, M.M., Stein, D.: Entropic cages for trapping DNA near a nanopore. Nat. Commun. 6, 6222 (2015). https://doi.org/10.1038/ncomms7222
37. Liu, X., Zimny, P., Zhang, Y., Rana, A., Nagel, R., Reisner, W., Dunbar, W.B.: Flossing DNA in a Dual Nanopore Device. Small. 16, e1905379 (2020). https://doi.org/10.1002/smll.201905379
38. Zhang, Y., Clausmeyer, J., Babakinejad, B., Cordoba, A.L., Ali, T., Shevchuk, A., Takahashi, Y., Novak, P., Edwards, C., Lab, M., Gopal, S., Chiappini, C., Anand, U., Magnani, L., Coombes, R.C., Gorelik, J., Matsue, T., Schuhmann, W., Klenerman, D., Sviderskaya, E.V., Korchev, Y.: Spearhead Nanometric Field-Effect Transistor Sensors for Single-Cell Analysis. Acs Nano. 10, 3214–3221 (2016). https://doi.org/10.1021/acsnano.5b05211
39. Steinbock, L.J., Bulushev, R.D., Krishnan, S., Raillon, C., Radenovic, A.: DNA Translocation through Low-Noise Glass Nanopores. ACS Nano. 7, 11255–11262 (2013). https://doi.org/10.1021/nn405029j
40. Ren, R., Zhang, Y., Nadappuram, B.P., Akpinar, B., Klenerman, D., Ivanov, A.P., Edel, J.B., Korchev, Y.: Nanopore extended field-effect transistor for selective single-molecule biosensing. Nat Commun. 8, 586 (2017). https://doi.org/10.1038/s41467-017-00549-w
41. Park, K.D., Lee, S.W., Takama, N., Fujii, T., Kim, B.J.: Arbitrary-shaped nanochannels fabricated by polymeric deformation to achieve single DNA stretching. Microelectron. Eng. 86, 1385–1388 (2009). https://doi.org/10.1016/j.mee.2009.02.003
42. Mills, K.L., Huh, D., Takayama, S., Thouless, M.D.: Instantaneous fabrication of arrays of normally closed, adjustable, and reversible nanochannels by tunnel cracking. Lab. Chip. 10, 1627–1630 (2010). https://doi.org/10.1039/C000863J
43. Chou, S.Y., Krauss, P.R., Renstrom, P.J.: Imprint of sub-25 nm vias and trenches in polymers. Appl. Phys. Lett. 67, 3114–3116 (1995). https://doi.org/10.1063/1.114851
44. Hong, S.M., Kim, S.H., Kim, J.H., Hwang, H.I.: Hydrophilic surface modification of PDMS using atmospheric RF plasma. J. Phys. Conf. Ser. 34, 656–661 (2006). https://doi.org/10.1088/1742-6596/34/1/108
45. Vesel, A., Mozetic, M.: Surface modification and ageing of PMMA polymer by oxygen plasma treatment. Vacuum. 6, 634–637 (2012). https://doi.org/10.1016/j.vacuum.2011.07.005
46. ONeil, C.E., Jackson, J.M., Shim, S.-H., Soper, S.A.: Interrogating Surface Functional Group Heterogeneity of Activated Thermoplastics Using Super-Resolution Fluorescence Microscopy. Anal. Chem. 88, 3686–3696 (2016). https://doi.org/10.1021/acs.analchem.5b04472
47. Zhang, D., Dougal, S.M., Yeganeh, M.S.: Effects of UV Irradiation and Plasma Treatment on a Polystyrene Surface Studied by IR−Visible Sum Frequency Generation Spectroscopy. Langmuir. 16, 4528–4532 (2000). https://doi.org/10.1021/la991353i

48. Chai, J., Lu, F., Li, B., Kwok, D.Y.: Wettability interpretation of oxygen plasma modified poly(methyl methacrylate). Langmuir ACS J. Surf. Colloids. 20, 10919–10927 (2004). https://doi.org/10.1021/la048947s
49. Puliyalil, H., Cvelbar, U.: Selective Plasma Etching of Polymeric Substrates for Advanced Applications. Nanomaterials. 6, 108 (2016). https://doi.org/10.3390/nano6060108
50. Tan, S.H., Nguyen, N.-T., Chua, Y.C., Kang, T.G.: Oxygen plasma treatment for reducing hydrophobicity of a sealed polydimethylsiloxane microchannel. Biomicrofluidics. 4, (2010). https://doi.org/10.1063/1.3466882
51. Tang, L., Lee, N.Y.: Micro-perforated elastomeric poly(dimethylsiloxane) mask fabricated using high-aspect-ratio micro-pillar arrays for spatially defined surface modification: an unconventional method for establishing a microarray platform. Anal. Bioanal. Chem. 394, 1227–1232 (2009). https://doi.org/10.1007/s00216-009-2781-1
52. Wu, W., Wu, J., Kim, J.-H., Lee, N.Y.: Instantaneous room temperature bonding of a wide range of non-silicon substrates with poly(dimethylsiloxane) (PDMS) elastomer mediated by a mercaptosilane. Lab. Chip. 15, 2819–2825 (2015). https://doi.org/10.1039/C5LC00285K
53. Ahn, S.Y., Lee, N.Y.: Solvent-free thermoplastic-poly(dimethylsiloxane) bonding mediated by UV irradiation followed by gas-phase chemical deposition of an adhesion linker. J. Micromechanics Microengineering. 25, 075007 (2015). https://doi.org/10.1088/0960-1317/25/7/075007
54. McCarley, R.L., Vaidya, B., Wei, S., Smith, A.F., Patel, A.B., Feng, J., Murphy, M.C., Soper, S.A.: Resist-free patterning of surface architectures in polymer-based microanalytical devices. J. Am. Chem. Soc. 127, 842–843 (2005). https://doi.org/10.1021/ja0454135
55. Wei, S., Vaidya, B., Patel, A.B., Soper, S.A., McCarley, R.L.: Photochemically Patterned Poly(methyl methacrylate) Surfaces Used in the Fabrication of Microanalytical Devices. J. Phys. Chem. B. 109, 16988–16996 (2005). https://doi.org/10.1021/jp051550s
56. Tsao, C.-W., Hromada, L., Liu, J., Kumar, P., DeVoe, D.: Low temperature bonding of PMMA and COC microfluidic substrates using UV/ozone surface treatment. Lab. Chip. 7, 499–505 (2007). https://doi.org/10.1039/b618901f
57. Jackson, J.M., Witek, M.A., Hupert, M.L., Brady, C., Pullagurla, S., Kamande, J., Aufforth, R.D., Tignanelli, C.J., Torphy, R.J., Yeh, J.J., Soper, S.A.: UV activation of polymeric high aspect ratio microstructures: ramifications in antibody surface loading for circulating tumor cell selection. Lab. Chip. 14, 106–117 (2013). https://doi.org/10.1039/C3LC50618E
58. Han, J., Lee, S., Puntambekar, A., Murugesan, S.: UV Adhesive Bonding Techniques in Room Temperature for Plastic Lab-On-A-Chips. 7th Lnternational Conf. Miniaturized Chem. Blochemlcal Anal. Syst. 4 (2003)
59. Sunkara, V., Park, D.-K., Hwang, H., Chantiwas, R., Soper, S.A., Cho, Y.-K.: Simple room temperature bonding of thermoplastics and poly(dimethylsiloxane). Lab. Chip. 11, 962–965 (2011). https://doi.org/10.1039/C0LC00272K
60. Nguyen, T.P.O., Tran, B.M., Lee, N.Y.: Thermally robust and biomolecule-friendly room-temperature bonding for the fabrication of elastomer–plastic hybrid microdevices. Lab. Chip. 16, 3251–3259 (2016). https://doi.org/10.1039/C6LC00751A
61. Jang, M., Park, S., Lee, N.Y.: Polycarbonate bonding assisted by surface chemical modification without plasma treatment and its application for the construction of plastic-based cell arrays. Sens. Actuators Phys. 206, 57–66 (2014). https://doi.org/10.1016/j.sna.2013.11.022

62. Zhang, H., Lee, N.Y.: Non-silicon substrate bonding mediated by poly(dimethylsiloxane) interfacial coating. Appl. Surf. Sci. 327, 233–240 (2015). https://doi.org/10.1016/j.apsusc.2014.10.172
63. Kovach, K.M., Capadona, J.R., Gupta, A.S., Potkay, J.A.: The effects of PEG-based surface modification of PDMS microchannels on long-term hemocompatibility. J. Biomed. Mater. Res. A. 102, 4195–4205 (2014). https://doi.org/10.1002/jbm.a.35090
64. Schnitzer, C., Ripperger, S.: Influence of Surface Roughness on Streaming Potential Method. Chem. Eng. Technol. 31, 1696–1700 (2008). https://doi.org/10.1002/ceat.200800180
65. Ellinas, K., Tserepi, A., Gogolides, E.: Superhydrophobic, passive microvalves with controllable opening threshold: exploiting plasma nanotextured microfluidics for a programmable flow switchboard. Microfluid Nanofluid. 10 (2014)
66. Jackson, J.M., Witek, M.A., Hupert, M.L., Brady, C., Pullagurla, S., Kamande, J., Aufforth, R.D., Tignanelli, C.J., Torphy, R.J., Yeh, J.J., Soper, S.A.: UV activation of polymeric high aspect ratio microstructures: ramifications in antibody surface loading for circulating tumor cell selection. Lab. Chip. 14, 106–117 (2014). https://doi.org/10.1039/c3lc50618e
67. Wang, C., Yan, Q., Liu, H.-B., Zhou, X.-H., Xiao, S.-J.: Different EDC/NHS Activation Mechanisms between PAA and PMAA Brushes and the Following Amidation Reactions. Langmuir. 27, 12058–12068 (2011). https://doi.org/10.1021/la202267p
68. Hermanson, G.T.: Bioconjugate techniques. Elsevier/AP, London ; Waltham, MA (2013)
69. Keleştemur, S., Altunbek, M., Culha, M.: Influence of EDC/NHS coupling chemistry on stability and cytotoxicity of ZnO nanoparticles modified with proteins. Appl. Surf. Sci. 403, 455–463 (2017). https://doi.org/10.1016/j.apsusc.2017.01.235
70. Oliver-Calixte, N.J., Uba, F.I., Battle, K.N., Weerakoon-Ratnayake, K.M., Soper, S.A.: Immobilization of Lambda Exonuclease onto Polymer Micropillar Arrays for the Solid-Phase Digestion of dsDNAs. Anal. Chem. 86, 4447–4454 (2014). https://doi.org/10.1021/ac5002965
71. Pham, D.T., Saelim, N., Tiyaboonchai, W.: Crosslinked fibroin nanoparticles using EDC or PEI for drug delivery: physicochemical properties, crystallinity and structure. J. Mater. Sci. 53, 14087–14103 (2018). https://doi.org/10.1007/s10853-018-2635-3
72. Han, J.-L., Xia, X., Tao, Y., Yun, H., Hou, Y.-N., Zhao, C.-W., Luo, Q., Cheng, H.-Y., Wang, A.-J.: Shielding membrane surface carboxyl groups by covalent-binding graphene oxide to improve anti-fouling property and the simultaneous promotion of flux. Water Res. 102, 619–628 (2016). https://doi.org/10.1016/j.watres.2016.06.032
73. Urban, P.L., Goodall, D.M., Bruce, N.C.: Enzymatic microreactors in chemical analysis and kinetic studies. Biotechnol. Adv. 24, 42–57 (2006). https://doi.org/10.1016/j.biotechadv.2005.06.001
74. Křenková, J., Foret, F.: Immobilized microfluidic enzymatic reactors. ELECTROPHORESIS. 25, 3550–3563 (2004). https://doi.org/10.1002/elps.200406096
75. Slovakova, M., Minc, N., Bilkova, Z., Smadja, C., Faigle, W., Fütterer, C., Taverna, M., Viovy, J.-L.: Use of self assembled magnetic beads for on-chip protein digestion. Lab. Chip. 5, 935–942 (2005). https://doi.org/10.1039/B504861C
76. Nel, A.L., Minc, N., Smadja, C., Slovakova, M., Bilkova, Z., Peyrin, J.-M., Viovy, J.-L., Taverna, M.: Controlled proteolysis of normal and pathological prion protein in a microfluidic chip. Lab. Chip. 8, 294–301 (2008). https://doi.org/10.1039/B715238H

77. May, O.: Biocatalysts and Enzyme Technology. By Klaus Buchholz, Volker Kasche and Uwe T. Bornscheuer. Angew. Chem. Int. Ed. 44, 5367–5367 (2005). https://doi.org/10.1002/anie.200585299
78. Lee, J., A. Soper, S., K. Murray, K.: Development of an efficient on-chip digestion system for protein analysis using MALDI-TOF MS. Analyst. 134, 2426–2433 (2009). https://doi.org/10.1039/B916556H
79. Ho Kang, S., Lee, S., S. Yeung, E.: Digestion of individual DNA molecules by λ-exonuclease at liquid–solid interface. Analyst. 135, 1759–1764 (2010). https://doi.org/10.1039/C0AN00145G
80. Zhang, J., McCabe, K.A., Bell, C.E.: Crystal structures of lambda exonuclease in complex with DNA suggest an electrostatic ratchet mechanism for processivity. Proc. Natl. Acad. Sci. U. S. A. 108, 11872–11877 (2011). https://doi.org/10.1073/pnas.1103467108
81. Lee, S., Kang, S.H.: Single-molecule DNA digestion in various alkanethiol-functionalized gold nanopores. Talanta. 107, 297–303 (2013). https://doi.org/10.1016/j.talanta.2013.01.046
82. Lee, S., Kang, S.H., Yeung, E.S.: Enzyme digestion of entrapped single-DNA molecules in nanopores. Talanta. 85, 2135–2141 (2011). https://doi.org/10.1016/j.talanta.2011.07.058
83. Novak, B.R., Moldovan, D., Nikitopoulos, D.E., Soper, S.A.: Distinguishing Single DNA Nucleotides Based on Their Times of Flight Through Nanoslits: A Molecular Dynamics Simulation Study. J. Phys. Chem. B. 117, 3271–3279 (2013). https://doi.org/10.1021/jp309486c
84. Clarke, J., Wu, H.-C., Jayasinghe, L., Patel, A., Reid, S., Bayley, H.: Continuous base identification for single-molecule nanopore DNA sequencing. Nat. Nanotechnol. 4, 265–270 (2009). https://doi.org/10.1038/nnano.2009.12
85. Alexa Fluor™ 594 Cadaverine, https://www.thermofisher.com/order/catalog/product/A30678
86. Suzuki, M., Ikeda, K., Yamaguchi, M., Kudoh, S.N., Yokoyama, K., Satoh, R., Ito, D., Nagayama, M., Uchida, T., Gohara, K.: Neuronal cell patterning on a multi-electrode array for a network analysis platform. Biomaterials. 34, 5210–5217 (2013). https://doi.org/10.1016/j.biomaterials.2013.03.042
87. Teare, D.O.H., Ton-That, C., Bradley, R.H.: Surface characterization and ageing of ultraviolet–ozone-treated polymers using atomic force microscopy and x-ray photoelectron spectroscopy. Surf. Interface Anal. 29, 276–283 (2000). https://doi.org/10.1002/(SICI)1096-9918(200004)29:4<276::AID-SIA740>3.0.CO;2-P
88. Scheicher, S.R., Krammer, K., Fian, A., Kargl, R., Ribitsch, V., Köstler, S.: Patterned Surface Activation of Cyclo-Olefin Polymers for Biochip Applications. Period. Polytech. Chem. Eng. 58, 61–67 (2014). https://doi.org/10.3311/PPch.7203
89. V. Nair, S., A. Witek, M., M. Jackson, J., M. Lindell, M.A., A. Hunsucker, S., Sapp, T., E. Perry, C., L. Hupert, M., Bae-Jump, V., A. Gehrig, P., Z. Wysham, W., M. Armistead, P., Voorhees, P., A. Soper, S.: Enzymatic cleavage of uracil-containing single-stranded DNA linkers for the efficient release of affinity-selected circulating tumor cells. Chem. Commun. 51, 3266–3269 (2015). https://doi.org/10.1039/C4CC09765C
90. Schultz, N., Metreveli, G., Franzreb, M., Frimmel, F.H., Syldatk, C.: Zeta potential measurement as a diagnostic tool in enzyme immobilisation. Colloids Surf. B Biointerfaces. 66, 39–44 (2008). https://doi.org/10.1016/j.colsurfb.2008.05.004

Vita

Qinhan Liu was born and raised in Xi'an, Shanxi, China. She completed her Bachelor of degree in Material Science & Engineering at Huazhong University of Science and Technology in June 2017. She joined the Department of Mechanical & Industrial Engineering at Louisiana State University in August 2018. She plans to graduate December 2021 for her master's degree from Louisiana State University. Her advisor is Dr. Sunggook Park and she focused on the fabrication and measurement of polymeric nanofluidic sensors.

.